

## CHAPTER 10: RF SYSTEMS

WOLFGANG ANDERS

*Helmholtz-Zentrum Berlin for Materials and Energy*

*Albert-Einstein-Str. 15, D-12489*

*Berlin, Germany*

AXEL NEUMANN

*SRF Science and Technology/BESSY II*

*Helmholtz-Zentrum Berlin for Materials and Energy*

*Albert-Einstein-Str. 15, D-12489*

*Berlin, Germany*

### Keywords

RF Transmitters, Tetrode, Klystron, Solid State RF Amplifier, Modulators, Transmission Line, Circulator, Low-level RF, RF Control System, Fundamental Power Coupler, Waveguide Coupler, Coaxial Coupler, Higher-Order Mode Coupler

### Abstract

The RF system is responsible for feeding adequate power to the injector with required phase and amplitude stability. The low level RF system provides the input for the high power amplifier and controls the phase and amplitude *via* feedback and feedforward loops. The high power RF amplifies the milliwatt level input to kilowatt/megawatt level. The first step in developing the high power RF system is to establish the power level and the tolerances required. In this chapter, we discuss the methods to determine these values followed by a description of the essential components, namely, the preamplifier, high power amplifier, transmission line, fundamental power couplers and higher order mode couplers. We describe major errors sources for field stability of the RF cavities such as frequency shift due to temperature fluctuation, Lorentz detuning, micro-phonics. We provide a sequence of steps to design and operate the LLRF a generic system with examples for controlling the LLRF.

This chapter is subdivided into six sections: After an introduction, we discuss the essential aspects of the high power RF transmitters and transmission lines, the low-level RF (LLRF) system and the issues related to the fundamental- and higher order mode-couplers.

## 10.1 OVERVIEW OF APPLICATIONS AND REQUIREMENTS

The high-power RF system of a photoinjector is responsible for feeding adequate power with the required stability into the accelerating RF cavity. It amplifies a signal in the milliwatt power range from the master oscillator to a typical power level, from kilowatts to a few megawatts, which is fed to the fundamental power coupler of the accelerating cavity. Its main components are the preamplifier, the tube or solid-state-based high power amplifier, with the corresponding power supplies and the transmission line, including a circulator. Depending upon its application, the RF system is designed for continuous wave (CW) or in pulsed operation mode.

The LLRF system is responsible for controlling the amplitude and phase *via* feedback loops and provides the input signal for the high power RF system. The feedback loops are realized either in analog technology or in digital technology based on field programmable gate-array processors.

An overview of fundamental- and higher order mode- (HOM) couplers for the RF cavities will complete this chapter. Fundamental power couplers (FPC) transmit high power levels from the transmission line into the cavity cell that is under vacuum. HOM couplers also damp unwanted frequency modes excited by the beam in the cavity cell. Fundamental mode and HOM coupler technologies differ significantly for normal conducting- (NC) and superconducting- (SC) cavities.

### Power Requirements

The application of an RF photoinjector determines the main design parameters of the corresponding RF cavity. The decision between normal or superconducting and between the pulsed or CW mode of operation determines the field-control strategy and also the coupling strength of the supplied forward power wave to the cavity. The coupling strength, in the absence of the beam, given by the ratio between external and intrinsic quality factor,  $Q_{ext}$  and  $Q_0$  respectively, finally gives the half-bandwidth  $f_{1/2}$  of the system expressed

$$f_{1/2} = \frac{f_0}{2Q_L} \quad (10.1)$$

with

$$Q_L = \left( \frac{1}{Q_{ext}} + \frac{1}{Q_0} \right)^{-1} \quad (10.2)$$

and,

$$Q_{ext} = \frac{\omega_0 U}{P_{ext}} \quad (10.3)$$

where  $Q_L$  is the loaded quality factor,  $f_0$  is the cavity's resonance frequency, and  $\omega_0$  the cavity's angular resonance frequency.  $Q_{ext}$  is the ratio of stored energy in a cavity,  $U$ , to the power  $P_{ext}$  leaking through the coupler in every RF period,  $\omega_0$ . Three factors drive the choice of  $Q_{ext}$ : The amount of beam current to be accelerated; the expected cavity detuning; and, the available power. The required power to establish a given accelerating field,  $V_{cav}$ , at a given  $Q_L$ , the geometric shunt impedance ( $R/Q$ ), the beam current  $I_b$  and accelerating phase  $\Phi_b$  is given by

$$P_f = \frac{V_{cav}^2}{4(R/Q)Q_L} * \left[ \left( 1 + \frac{(R/Q)Q_L I_b}{V_{cav}} \cos(\Phi_b) \right)^2 + \left( \frac{\Delta f}{f_{1/2}} + \frac{(R/Q)Q_L I_b}{V_{cav}} \sin(\Phi_b) \right)^2 \right] \quad (10.4)$$

Besides the beam loading, power is determined by the cavity's detuning,  $\Delta f$ , over the cavity's half-bandwidth,  $f_{1/2}$ . This relationship is of major concern for narrow-band superconducting cavities wherein the amount of detuning, especially for pulsed operation, easily exceeds the cavity's bandwidth. On the other hand, the selection of the coupling impacts the field's stability.

The field's phase stability,  $\sigma_\phi$ , is given by the cavity's frequency detuning,  $\sigma_f$ , and  $f_{1/2}$

$$\sigma_\phi = \arctan\left(\frac{\sigma_f}{f_{1/2}}\right) \quad (10.5)$$

Figure 10.1 shows the required RF power due to microphonic noise. We depict the RF power versus the cavity's bandwidth for different microphonic noise levels for a SC cavity used in a low current application with 2 kW beam loading. The RF power required for stable operation is a multiple of the beam loading. Piezo actuator-based fast cavity tuning loops can compensate for part of the microphonic detuning in attempting to minimize the RF power of the installation, but it is challenging to design these loops [10.1].

When specifying the overhead transmitter power, we also must take into account the losses in the transmission line and in the circulator, in addition to losses in the cavity's walls, beam loading and microphonic needs.

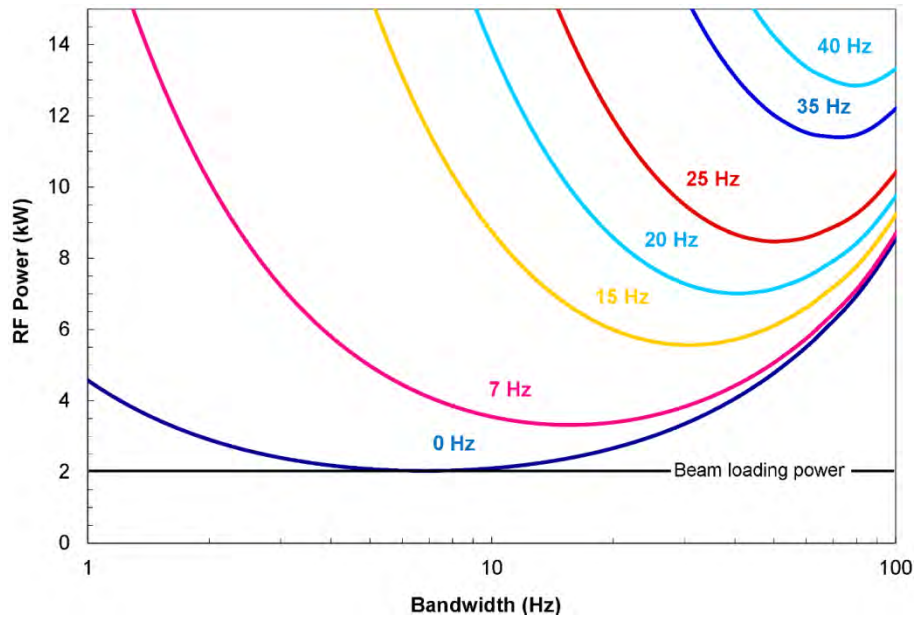


Figure 10.1. Required RF power to compensate for microphonics for a TESLA cavity operating at  $20 \text{ MV m}^{-1}$ . Depicted is the RF power versus the cavity bandwidth for different microphonic noise levels a system with 2 kW beam loading. The RF power required for stable operation is significantly more than that for the beam loading. [Courtesy of J. Knobloch]

Three different categories define the power level required in photoinjector application:

- CW or pulsed operation
- normal conducting or superconducting cavity
- beam currents below or above 1 mA

CW operation is used for the low energy, superconducting free electron laser (FEL) [10.2] and the Energy Recovery Linac (ERL) [10.3], while pulsed operation is chosen for applications with normal conducting linac structures [10.4], [10.5]. Pulsed high energy FEL accelerators with a superconducting linac [10.6] nowadays are equipped with a NC pulsed gun cavity [10.7]. Because gun cavities are operated with high accelerating gradients to preserve the emittance, normal conducting gun cavities require RF power at megawatt levels, as achieved in pulsed operation. Superconducting gun cavities generally are operated in the CW mode. The wall losses in superconducting cavities amount to a mere few watts. Beam loading and

microphonic detuning define the power level of the transmitter. Special injectors for high current ERLs with beam currents of 100 mA to 1 A need transmitters with power levels over 100 kW [10.3], [10.8], [10.9]. This breaks down the transmitters into three categories:

- CW transmitter < 50 kW for SC injector cavities with low beam loading
- CW transmitter > 50 kW for SC injector cavities with high beam loading
- pulsed transmitters at megawatt power levels for NC injector cavities

For CW transmitters operated below 50 kW, solid-state technology and inductive output tubes (IOTs) are good choices. For CW operated transmitters above 50 kW, klystron and IOT tubes are competing concepts, while pulsed megawatt power-level transmitters are realized with klystrons. However, we note that progress in technology will increase the power level for economic applications of solid-state transmitters.

## 10.2 TRANSMITTERS

The transmitter is the device that amplifies the milliwatt level RF signal from the low-level RF system to the kilowatt- or megawatt-power level. The following are the major components of a transmitter:

1. preamplifier
2. power stage
3. set of power supplies
4. interlock systems
5. control system
6. cooling system

This section describes the most relevant devices for the several power stages. We show, using the example of a CW operated IOT transmitter, how to specify the stability of the power supplies from the general specifications of the transmitter and the data of the power stage. For pulsed transmitters, we detail the different circuit principles for the power modulators. We briefly mention the preamplifier and other auxiliary systems.

### 10.2.1 Power Stage

The power stage is the dominant part of a RF system. In the past century, high-power RF was generated only by electron tubes, such as tetrodes, klystrons and IOTs. Solid-state technology became much more relevant with the increase in the power levels and efficiency of single RF transistors that, in turn, resulted in an increasing range of economical RF-transmitter solutions.

The efficiency and harmonic content of the output signal of a power amplifier depend on which one of the three classes of operation is employed, *i.e.*, A, B, or C: In class-A operations, the active element conducts throughout the whole RF cycle. Its harmonic content is low and its linear amplification range is high; the drawback is a low efficiency, especially during partial load operation. Even without any input signal, power is wasted. Class-A operation is used with klystrons.

In class-B operations, the amplifier is conducting only during the positive half of the RF cycle. Here, the efficiency is higher than in class-A, but so is the harmonic content. In class-C operations, less than half of the positive RF cycle is used, yielding a very high harmonic content and the highest efficiency; however, there is no longer a linear dependence of the output signal to the input.

Tetrodes, IOTs and solid-state amplifiers usually are employed in a mix of class-A and class-B, compromising between the harmonic content, the linear behavior of the amplification and high efficiency.

### 10.2.1.1 Tetrode

Tetrodes are mostly used at frequencies below 200 MHz. Figure 10.2 is a schematic of a tetrode. The anode and screen grid are at a positive potential, and the control grid at a negative potential with respect to the cathode. The control grid determines the intensity of the beam in the tetrode, while the screen grid prevents capacitive feedback from the anode to the control grid.

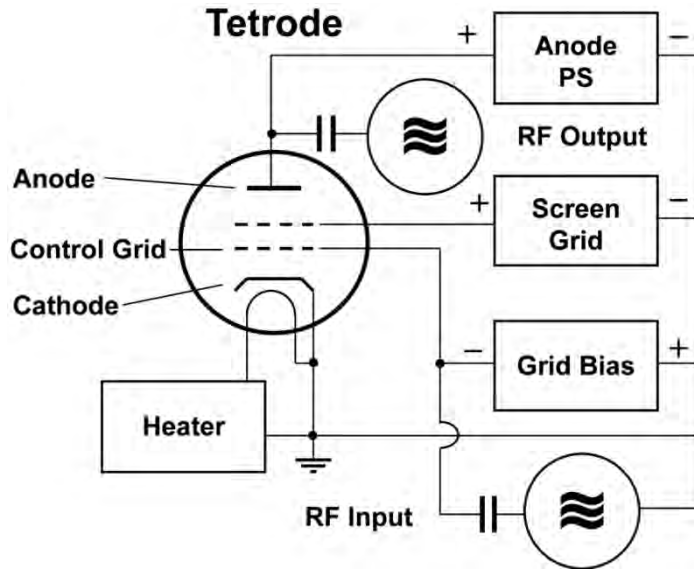


Figure 10.2. Schematic diagram of a tetrode. The RF input controls the current from the cathode to the anode via the grid voltage.

The RF tetrode has a coaxial design, with the cathode inside and the anode outside, allowing for effective cooling of the anode. Output power is limited by the maximum current density available from the cathode and the maximum power that can be dissipated from the anode. The dimensions and spacing of the electrodes are limited to avoid

- Variation in signal levels – the length of the anode must be less than the free space wavelength of the signal to be amplified.
- Higher order modes between the anode and the screen grid – the perimeter of the anode must be less than the free-space wavelength.
- Transient time problems – spacing between the anode and cathode must be less than the RF period. Increasing the anode potential to overcome this problem may cause discharge between the electrodes.

The coaxial design of the tetrode allows the construction of coaxial input and output circuits. The most common arrangement is a grounded control grid. The input- and output-circuits are well isolated because both grids are at RF ground. However, as the anode current flows in the input circuit, both the input impedance and the gain are lower than for a grounded cathode.

### 10.2.1.2 Klystron

The klystron is a vacuum electron tube with a linear output-input characteristic. Figure 10.3 is a schematic diagram of a four-cavity klystron; the main parts of which are:

1. an electron gun to produce the high current electron beam
2. a set of cavities to modulate the velocity of the beam
3. an RF input coupler at the first cavity

4. an RF output coupler at the last cavity
5. an axial magnetic field to confine the electron beam, usually generated by a solenoid electromagnet
6. the collector for the spent electrons

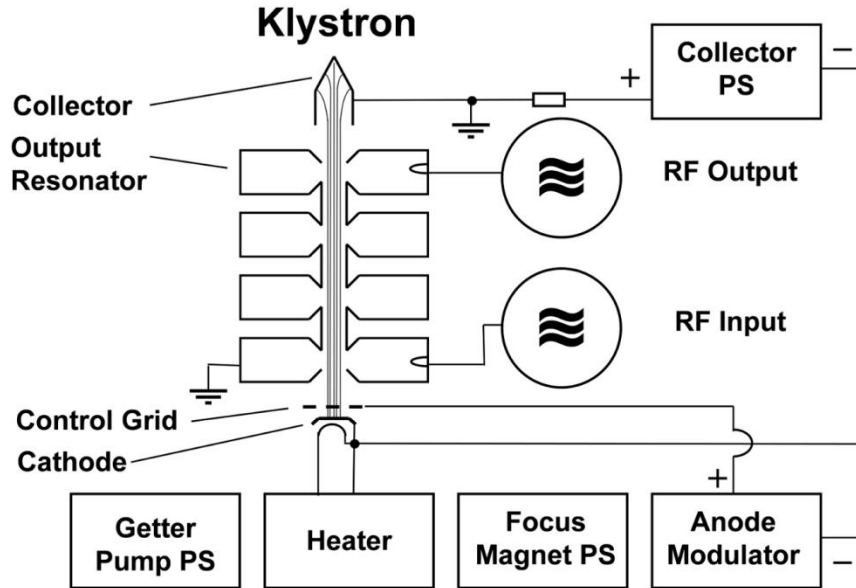


Figure 10.3. Schematic diagram of a four-cavity klystron showing the electron gun area with the cathode, the set of cavities including the input cavity with an RF coupler, and the output cavity with the RF output. The solenoid magnet (not shown) along the klystron focuses the beam and the collector gathers up the spent beam.

The DC electron beam, produced in a thermionic electron gun, is accelerated by the voltage between the cathode and the collector. Typical voltages range from tens of kilovolts for small klystrons, up to hundreds of kilovolts for klystrons at the megawatt power-level. The electron beam passes through a cavity resonator excited in the  $TM_{010}$  mode, establishing an axial electric field across the gap in the drift tube. Depending on its phase, the RF field in the cavity accelerates or delays the electrons as they cross it. On leaving the cavity, the electron beam is velocity-modulated. After a particular length of drift tube, the “slow” electrons are caught up by the faster ones, causing current modulation. If a cavity is placed at this point, the electron beam induces an RF field in it. By using several cavities (typically four to seven) and by tuning them in a special way to frequencies slightly above and below the RF frequency, the current modulation can be optimized. Such tuning also determines the bandwidth of the klystron. The output cavity is placed at the point of maximum current modulation, thus inducing a high electric RF field. The output coupler extracts the power from the cavity. The typical efficiency of a klystron is 40-65% with respect to the DC beam power.

The beam is collimated in the tube by solenoid magnets to minimize losses into the klystron walls. This is essential because the power stored in the beam, if misdirected, could easily melt the walls of the tube. The spent beam is collected in the high power collector.

In a linear (class-A) operation mode, the output power is nearly linear with respect to the input power at constant collector voltage, but the gain of the tube falls when the drive power is increased beyond the level at which maximum output power is reached. Therefore, it is necessary to limit the drive power to avoid oscillations of the amplitude loop. During operations with too high input power, the electrons of the beam might be accelerated back and could damage the cathode.

Megawatt range (especially in pulsed operation) klystrons mostly are operated in saturated operation mode to run the tube at its maximum efficiency. Here, the input power of the klystron is set on a level in which the klystron is operated in saturation. A variation in the drive power will not affect the output. In saturated operation mode, the output power level of the klystron is adjusted by changing the collector voltage.

Klystrons have undergone considerable development and can be designed for a high frequency and output power range. The gain of a klystron typically is 40-55 dB; hence, the driver amplifier has to deliver only a few watts of power.

### 10.2.1.3 Inductive Output Tube

The inductive output tube (IOT) was invented in the late 1930s by A. Haeff [10.10] and L. Nergaard [10.11] a few years before the principles of the klystron were known. The IOT is a gridded tube, like a triode with an additional output resonator. The technology needed to build a high power IOT was not ready then, so velocity-modulated tubes, like the klystron, became popular as power RF amplifiers. In the late 1970s, progress in technology brought the IOT back into focus, and at the turn of the millennium, it became the most dominant TV transmitter tube. Figure 10.4 is a schematic of an IOT amplifier.

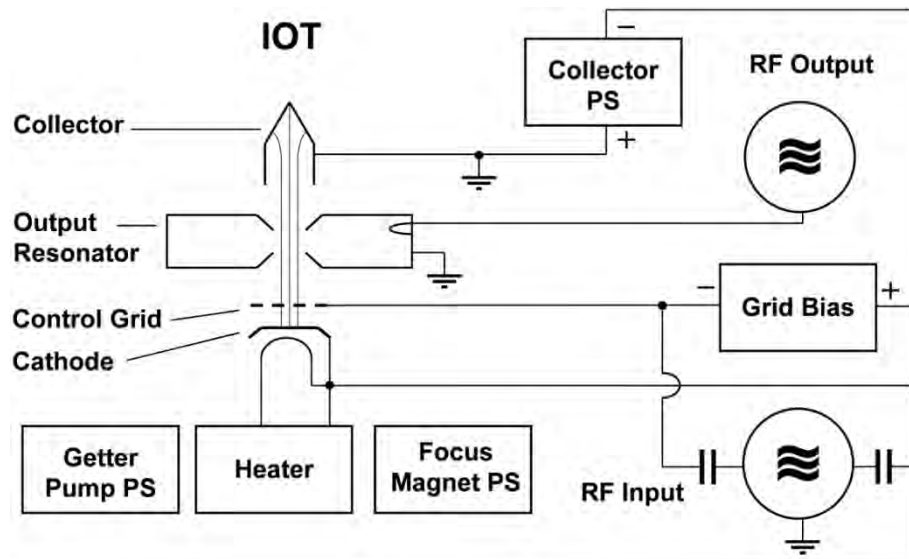


Figure 10.4. Schematic of an IOT. The DC electron beam, produced in a gun and modulated by a grid, induces an RF field in the cavity. The power of this field is coupled by an output coupler to the transmission line. The solenoid magnet (not shown) along the IOT focuses the beam and the collector intercepts the spent beam.

The IOT has five main parts:

1. an electron gun that generates the high current electron beam
2. a grid to modulate the density of the beam
3. an RF output coupler at the output cavity
4. an axial magnetic field, usually from an electromagnet, to confine the electron beam
5. the collector for the spent electrons

The DC electron beam, produced in a thermionic electron gun, is accelerated by the voltage of the collector's high voltage power supply. The electron beam passes through a grid biased such that the beam current flows only during the positive half of the input RF cycle. The bunched beam induces an RF field in the output resonator loaded by the output coupler. A solenoid magnet focuses the electrons in the tube. The high power collector gathers up the spent electrons. The input operation is similar to that of a tetrode, while the output operation resembles that of a klystron. Hence, some people refer to this device as a "klystrode."

Advantageously, the design of the IOT is simpler than that of a klystron, and it is smaller, easier to handle and weighs less. It is operated in class-AB mode, assuring good efficiency over a large dynamic range even though its typical maximum efficiency of ~65% is achieved only at the maximum power level. The class-AB operation makes the IOT a good choice (in terms of overall efficiency) in all systems with amplitude modulated applications, such as microphonic dominated operation of superconducting cavities. The major drawback of an IOT is its low gain, typically 23 dB, thus requiring a high power preamplifier, which raises the cost of an IOT-based transmitter.

#### 10.2.1.4 Solid-State Amplifiers

Solid-state technology for radio frequency power applications still is under development [10.12]. The critical issue is that the heat produced in the small crystal must be conducted properly to the cooling structures. Figure 10.5 depicts the maximum achievable RF power by one transistor, and its efficiency versus frequency.

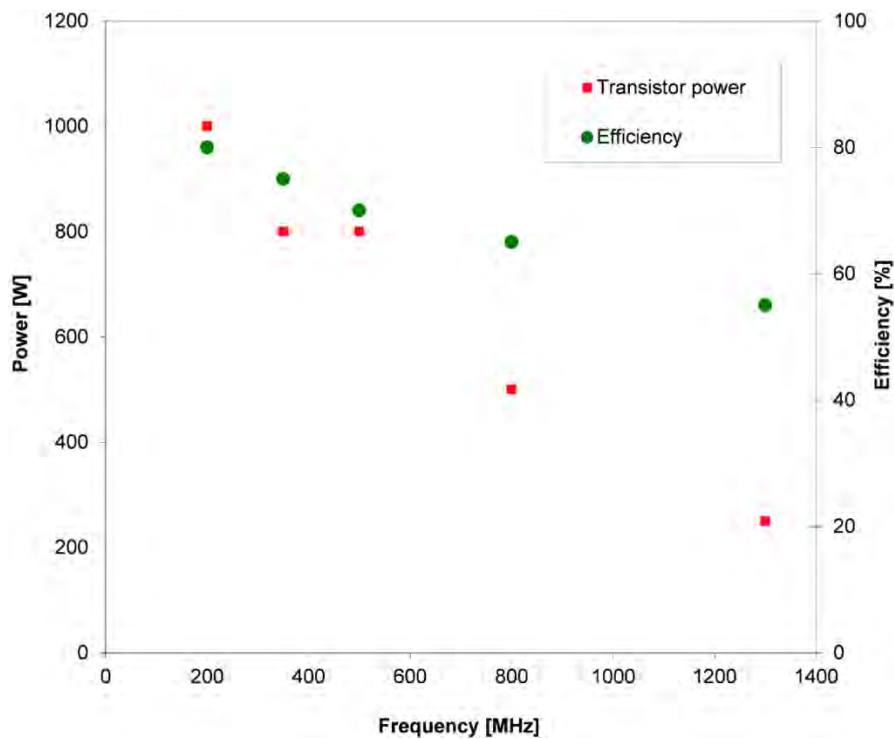


Figure 10.5. Maximum achievable RF power of a single transistor, and its efficiency versus frequency.

Obviously, in constructing a solid-state, high power RF amplifier, the power of tens or hundreds of RF transistors must be combined, as illustrated in Figure 10.6. Consequently, multiple power combiners are needed. New ideas utilize cavity combiners to add the power of up to a hundred modules in one device [10.13]: to date, this has been demonstrated only for a combiner with two inputs [10.14].

Adding up the power of a large number of transistors is the big advantage of solid-state technology, creating a modular system with high redundancy, and therefore high reliability. A tube failure in a klystron or IOT transmitter, where the generation of RF power is localized in one tube, shuts down the whole transmitter. With an appropriate modular design, only one part of the transmitter is shut down in such a failure and the overall transmitter continues operating on a reduced power level. The defective power supply or RF module can be changed during the following maintenance cycle. Depending on the construction, it may even be possible to change modules while the system is operating, leading to a high reliability of the transmitter.

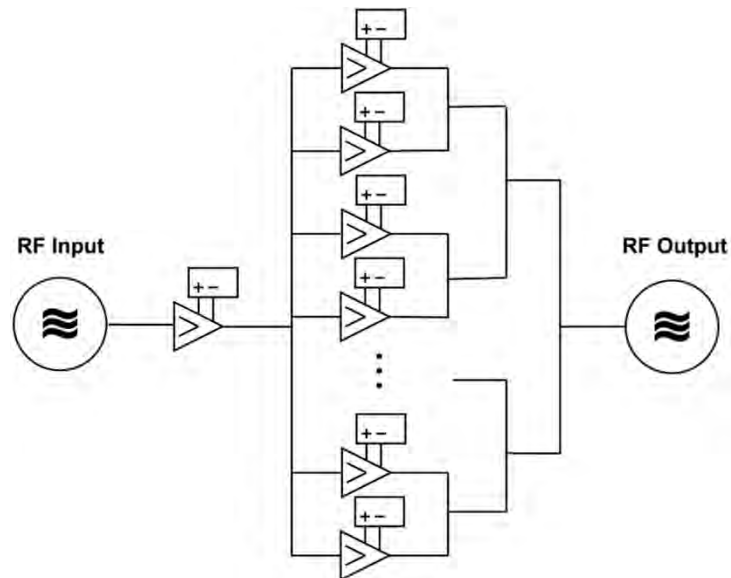


Figure 10.6. Schematic diagram of a solid-state amplifier. Up to a few hundred medium power amplifier modules are combined in a cascade. Combiners have a high number of inputs that reduces the depth of the cascade. Each amplifier module has its own power supply, assuring a high degree of redundancy.

The SOLEIL storage ring (Paris, France) contains a 354 MHz, 180 kW transmitter built from 315 W modules each powered by their own 600 W switched power supply [10.12]. It has operated for over 20 000 hr without a single RF power trip.

In contrast to electron tubes that need a set of several high voltage power supplies, solid-state RF modules need merely one low voltage power supply. RF transistors built in or before 2008 have been operated typically with a 28 V supply voltage. The new generation transistors operating at 50 V and thereby reducing the currents make solid-state technology easier to handle at high power levels.

Most RF modules are equipped with their own circulator, including a load to protect the transistor against reflections. The most significant drawback of solid-state technology is its restricted overall efficiency, including the combiner network, which still falls short of the values of electron tubes. Furthermore, given the complexity of the combiners, the price of a transmitter is only competitive to electron tubes at lower power levels and low frequencies. The answer to this problem is developing transistors with more power per single device.

### 10.2.2 Preamplifiers

Solid-state preamplifiers most often are those commercially available. Since the typical gain of a klystron is ~40-55 dB, the preamplifier power level ranges from 5 W for a 50 kW for CW klystron transmitter, to 500 W for a pulsed 20 MW system. The preamplifier for an IOT transmitter must be more powerful because the IOT's gain is only 20-23 dB. In a solid-state transmitter, the preamplifier is integrated. It is essential to specify and measure the noise of the preamplifier as carefully as the main power stage! Many amplifiers on the market, commonly used by the telecommunication industry, meet the required power level; however, most do not fulfill the stability requirements. By exchanging the integrated power supply for a more stable one, these amplifiers serve well in the RF systems of accelerators.

### 10.2.3 Power Supplies for CW Transmitters

The typical application of photoinjectors is in accelerators with short electron bunches that need very stable RF conditions. Typical specifications for the stability of the RF voltage in the cavity are  $0.1^\circ$  in phase and

0.1% in amplitude, or better. To reduce the load on the amplitude and phase loops of the LLRF system, the design of the transmitter should ensure that the noise of the RF at its output meets these requirements without using a loop. With the recent substantial progress in the development of switched power supplies, it is possible to realize this by carefully specifying the stability of the power supplies.

In this section, we discuss the transmitter's specifications using the example of an IOT amplifier [10.15]. The specifications for a klystron or tetrode transmitter are similar because the set of power supplies is alike, as evident by juxtaposing the power supplies in Figure 10.2, Figure 10.3 and Figure 10.4. We do not discuss here the specification of solid-state transmitter power supplies. However, stability issues, particularly dynamic stability, can be applied in the same way.

### ***10.2.3.1 Transfer Characteristics of the Electron Tube***

To translate the given specification in phase and amplitude stability into specifications of voltage stability for the power supplies, we must know the transfer characteristics of the IOT in amplitude and phase in relation to the different power supplies. These parameters must be provided by the manufacturer of the tube, or must be measured on a prototype.

Figure 10.7 illustrates the dependencies of phase and gain for voltage changes of the collector and the grid power supply for a 1.3 GHz, 16 kW IOT (Type E2V IOT116LS), as an example. The phase gain versus the collector voltage amounts to  $7^\circ$  per kilovolt at the most. Hence, for a phase stability specification of  $0.1^\circ$  maximum, the voltage stability should not exceed 15 V or  $6 \times 10^{-4}$  at 23 kV.

Looking at the requirements for voltage stability in relation to the amplitude stability of the transmitter, the gain variation versus the voltage of the collector's power supply is  $0.5 \text{ dB kV}^{-1}$ . To achieve a stability of 0.1% in amplitude, the voltage variation of the collector's power supply should not exceed a value of 8 V or  $3 \times 10^{-4}$  at 23 kV. The requirements for the amplitude stability are the more stringent; hence, the specification for the stability of the collector power supply should be better than  $3 \times 10^{-4}$ .

The same logic applies to the grid power supply. The gain stability gives the stronger specification, resulting in requirement for the grid bias of  $7 \times 10^{-4}$ . We note that the grid power supply is on a high voltage level that entails a greater effort in installation. However, if the grid power supply is applied to ground level, the noise of the collector power supply must be added to it, leading to much stronger specifications for the collector's power supply!

### ***10.2.3.2 Static- and Dynamic-Stability of the Collector Power Supply***

The collector's power supply is a high voltage power supply operated on ground level in the voltage regulation mode. The class-AB operation mode of the IOT causes variable beam currents depending on the power level of the RF output, necessitating a dynamic specification of the voltage stability. In Figure 10.8, we depict the collector voltage while pulsing the RF [10.15]. The details of the ripple are evident when the magnification is increased (zooming in), as are the overshoots. By varying the slope of the pulse, information is gained that is dependent on the bandwidth. With an exact specification, the manufacturer of the power supply can design it to meet the desired requirements.

It is advisable to limit the output current and voltage in the power supply. To reduce the thermal stress on the tube when switching on, the voltage should be ramped up in a few seconds, thereby extending the lifespan of the tube. Stored energy at the output of the power supply and discharge time should be specified according to the manufacturer's standards. A "wire-test" is usually specified to demonstrate the fulfillment

of the specifications. In this test, a thin wire (~0.2 mm) should not be destroyed when it shorts the output of the power supply.

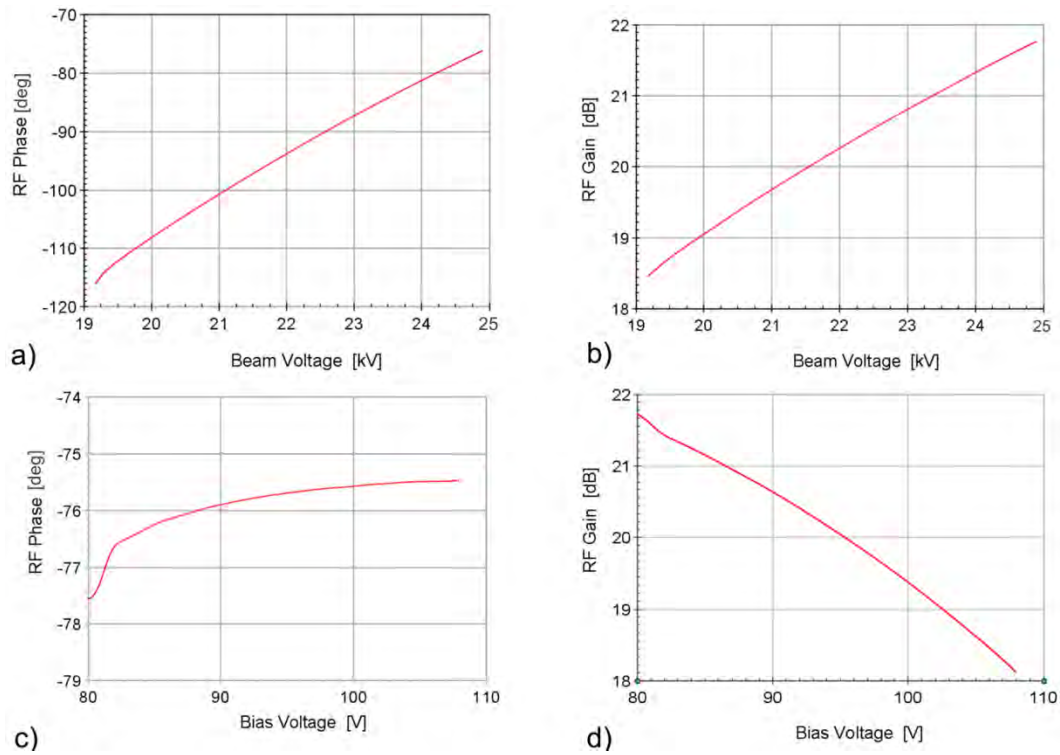


Figure 10.7. Transfer characteristics of E2V IOT116LS IOT: a) Depicts the phase shift; b) the amplitude gain versus collector voltage; c) depicts the phase shift; and d) the amplitude gain versus grid bias voltage.

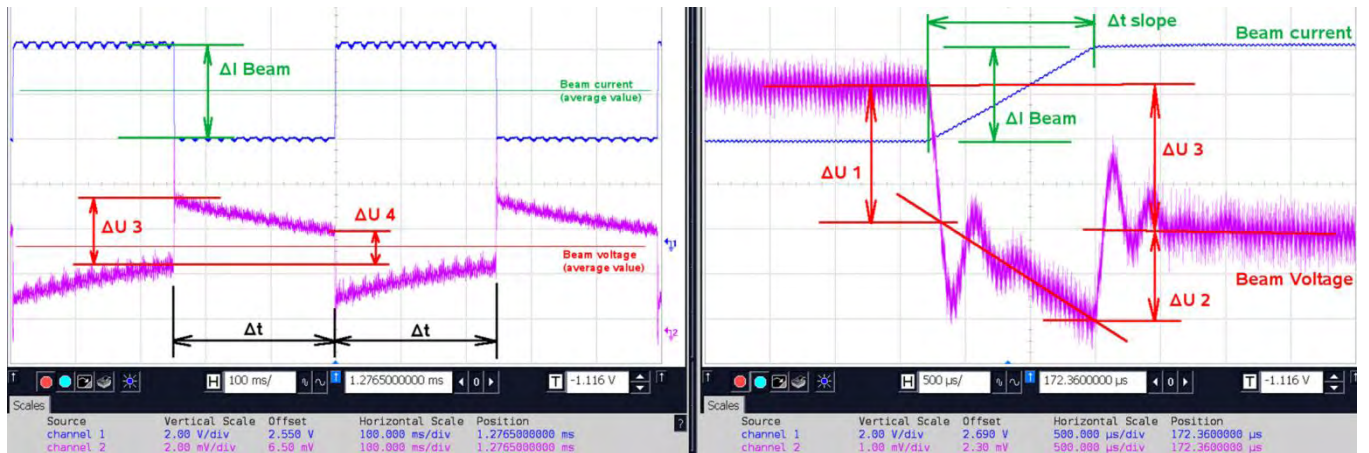


Figure 10.8. Voltage of the collector power supply of an IOT transmitter shown on an oscilloscope. Blue represents the beam current in the IOT and purple is the AC component of the collector voltage. When the beam current is abruptly changed ( $\Delta I_{Beam}$ ) by changing the RF drive power, the voltage regulation of the power supply is not able to follow instantly, resulting in a voltage step  $\Delta U$ . The right picture is a zoomed view of a rising edge of the RF. By varying the rise-time of the current, characteristics of the power supply can be determined. [[10.15]; Adapted under Creative Common Attribution 3.0 License ([www.creativecommons.org/licenses/by/3.0/us/](http://www.creativecommons.org/licenses/by/3.0/us/)) at [www.JACoW.org](http://www.JACoW.org).]

### 10.2.3.3 Stability of the Grid-Bias Power Supply

The grid-bias power supply is operated at the high voltage potential of the collector power supply in the voltage-regulated mode. It should have a low impedance, otherwise instabilities can occur in the tube: a

capacitor at the grid will help to maintain stability. Installing a current limiter, acting on the drive power of the tube, is recommended. In typical operation, the power supply is operated as a current drain, but for ion- or grid-emissions, it also must serve as a current source, hence, the grid bias power supply should be bipolar. The dynamic requirements and the discharge characteristics are the same as the collector power supply.

#### 10.2.3.4 Heater, Focusing and Getter Pump

The other power supplies do not need the same strict specifications as the collector and the grid bias power-supplies. Nevertheless, some special issues must be considered.

The heater's power supply should be either voltage- or current-regulated, operating on ground potential; the latter is gentler on the heater when switching on the power supply, and the internal resistance of the heater is very low. The heater should always be powered by a DC source. Even though thermionic emission is a slow process, a 50-60 Hz powered heater definitely influences the stability of the RF output. The heater is integrated in a system operated with a high voltage. Therefore, precautions should be taken to ensure that the power supply is protected from arcing.

The power supply for the focusing element is current-regulated and responsible for powering the magnet to focus the beam inside the tube. If focusing is switched off, the beam hitting the walls of the IOT can destroy the tube. Therefore, a fast interlock must be activated if the current in this power supply is out of a defined current window.

The power supply to the getter pump does not require special voltage stabilization. It must be protected against arcs in the tube and should generate an interlock signal if the current exceeds a defined threshold, indicating that the vacuum pressure in the tube is too high.

An example of two IOT based transmitters is shown in Figure 10.9 [10.15] operated at the HoBiCaT facility at the Helmholtz-Zentrum Berlin (HZB). Left is the 30 kW, 1.3 GHz system operated at the HoBiCaT facility. The right picture shows the 80 kW, 500 MHz transmitter operated at the Metrology Light Source (MLS) [10.16]. As the voltage of the collector power supply is 41 kV, the high voltage part of this power supply is built in an isolating oil tank. The concept, specifications and controls of both transmitters are the same.



Figure 10.9. Example of two IOT based transmitters. On the left is a 30 kW, 1.3 GHz system operated at the HoBiCaT facility at the Helmholtz-Zentrum Berlin. On the right is an 80 kW, 500 MHz transmitter operated at the MLS. [[10.15]; Adapted under Creative Commons Attribution 3.0 License ([www.creativecommons.org/licenses/by/3.0/us/](http://www.creativecommons.org/licenses/by/3.0/us/)) at [www.JACoW.org](http://www.JACoW.org).]

### 10.2.4 Modulators for Pulsed Transmitters

Pulsed RF systems are used in high power systems with klystrons, most of which run on megawatt peak RF power levels in the pulse. An overview on different techniques is given in [10.17]. Typical parameters for a modulator are [10.18]

Parameter [units]	Value
Pulse Voltage [kV]:	100-500
Pulse Current [A]:	50-500
Pulse Length:	
- Short Pulse [ $\mu\text{s}$ ]:	1-50
- Long Pulse [ $\mu\text{s}$ ]:	50 to some 1000
Repetition Rate [Hz]:	1-1000

Table 10.1. Typical parameters of a klystron modulator.

#### 10.2.4.1 Design principles

A typical pulse modulator consists of

- capacitor bank for storing energy
- charging unit for the capacitor bank
- switching unit
- voltage pulse transforming unit
- pulse-forming network (PFN)
- general control and interlock systems
- klystron as load

The energy storage usually is a capacitor-based system. The requirements on the capacitors should include the ability to handle the extremely high currents and high frequency transients for the short rise-and-fall times of the pulses. Low inductance, and sometimes even cooling, is needed to handle the energy flow characteristic of high repetition rate systems. The voltage drop on the capacitor within the pulse is a main contribution to the instability of RF power in the cavity. The required capacitance can be calculated directly from the maximum allowed voltage drop. The charging units are power supplies providing the average power needed to recharge the energy storage system between two pulses. The switching unit dominates the design of a modulator. There are two basic choices for it:

- systems that switch only ON
- systems that switch ON and OFF

An ON-switch device suffices for storage systems such as a PFN, or if the load defines the pulse length. In the past 50 years, gas switches, like thyratrons, generally were used, but recently high power semiconductors became increasingly common. Solutions were found by combining a series of GTOs (gate turn-off thyristor) and GCTs (gate-commutated thyristor) operated up to 4.5 kV.

In other cases, an ON/OFF-switch device, like MOSFETs, IGBTs, or IGCTs must be used; sometimes saturable magnet cores are employed as an additional switch element.

The limits of all these switch devices lie in their voltage, current and repetition rate. Nowadays, semiconductors are limited to 6.5 kV in voltage and 3 kA in pulse current, so that switch devices must be

combined for the input power of a klystron. Figure 10.10 shows three different design principles and circuits.

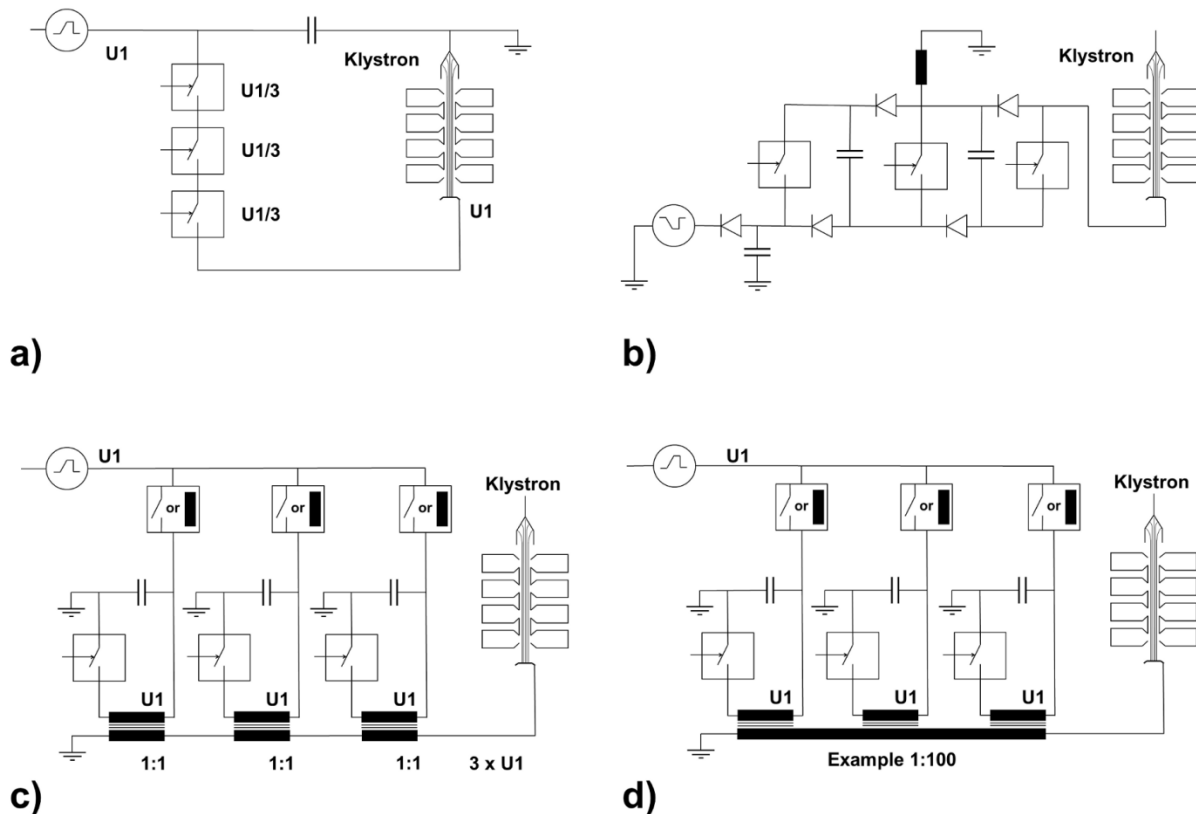


Figure 10.10. Different design principles for klystron modulators [10.18]: (a) Direct switch; (b) Marx Generator; and, (c) and (d) two inductive adders of different designs. [Courtesy of J. Knobloch]

#### 10.2.4.2 Direct Switch

In principle, it is possible to switch (Figure 10.10(a)) the whole voltage with a serial combination of switches to the load. The big challenge is in synchronizing the trigger circuits for each switch. This assembly requires a DC power supply with full-load voltage [10.19].

#### 10.2.4.3 Marx Generators

The Marx generator (Figure 10.10(b)) also is a serial combination of switching cells [10.20]; their main components are the switch and the capacitor. All devices work at the load voltage divided by the number of cells. Consequently, the power supply also is designed in the low kilovolt region. The disadvantage of a Marx generator is that it only allows a negative pulse voltage.

#### 10.2.4.4 Inductive Voltage and Inductive Current Adder

The voltage adder has a secondary coil to each primary coil. The output voltage in Figure 10.10(c) is the sum of all group windings transformed from the primary side [10.21]. The output current is the same as that of the primary coil. Typically, a 1 to 1 ratio is used to achieve a low inductance. The input voltage equals the output voltage divided by the steps, and therefore can be reduced down to kilovolts.

The current adder (Figure 10.10(d)) has one secondary coil to all primary winding coils. The ratio could be higher than 1:100, so the voltage is transformed *via* the winding relation. The power supply has the same specifications as the voltage adder type.

#### 10.2.4.5 Pulse Forming and Bouncers

The switch technology provides flexibility in the pulse length dynamic. However, the transformers from the core design are optimized to one specific pulse length and rise time. This means that we do not have a pulse-transformer concept for pulse length covering the range from microseconds to some milliseconds. Hence, there is a separation between short and long pulse modulators, especially with respect to the transformer design. Concepts for pulse shape and pulse qualities also differ:

- Passive pulse forming: PFNs are a combination of capacitors and tunable coils.
- Active pulse forming: Control circuit or with a secondary bounce-circuit against the droop.

Figure 10.11 [10.19] shows the modulator built by Puls-Plasmatechnik, Dortmund (PPT) [10.22] for feeding the 10 MW (Thales TH1801) multi-beam klystron. The modulator is constructed of a switched capacitor bank using a series stack of IGCTs with bouncer droop compensation and pulse transformer matching of 1:12. It can switch a 12 kV pulse voltage and 2 kA pulse current. The pulse width of the modulator can be varied from 50  $\mu$ s to 2 ms. For pulse lengths less than 1 ms, a smaller pulse transformer will yield better rise and fall times.



Figure 10.11. Klystron modulator built by PPT to operate the Thales TH1801, a 10 MW multi-beam klystron. The modulator consists of a capacitor bank using a series stack of IGCTs with bouncer droop compensation and pulse transformer matching of 1:12. It can switch a 12 kV pulsed voltage and 2 kA pulsed current. The pulse width can be varied from 50  $\mu$ s to 2 ms. [[10.19]; Adapted under Creative Common Attribution 3.0 License ([www.creativecommons.org/licenses/by/3.0/us/](http://www.creativecommons.org/licenses/by/3.0/us/)) at [www.JACoW.org](http://www.JACoW.org).]

#### 10.2.5 Other Parameters to be Specified for an RF Transmitter

The following list contains the main parameters for the general infrastructure of each transmitter, which must be defined.

- fast interlock, acting in the 100  $\mu$ s range
- connection to radiation-protection interlock
- connection to cavity signals
- interface to control system, type of PLC (programmable logic controller)

- accelerator control system interface
- metering instruments
- analog signals
- (water) cooling
- stability of mains
- temperature and humidity
- acceptable level of acoustic vibration

We emphasize a few of these points.

There are some expensive devices involved in a transmitter, so there is a need for installing fast-acting protection circuits because the reacting time of the PLC is insufficient. A fast, hard-wired interlock therein switches off the RF power *via* a PIN switch within microseconds. Other such emergencies include the following: Too high a reflection at the tube's output; voltage on the focusing magnet out of range; too high a drive power; arcs in the circulator, a transmission line, or the coupler of the cavity; too high a voltage in the cavity; or, bad vacuum in the cavity or in the radiation-safety interlock.

A second point is defining the internal control system, the analog measuring sockets, the metering instruments, and (often debatable) the interface to the accelerator control system. It always is worthwhile to define all signals which are required to be transmitted to the control system.

We highlight a final point, *viz.*, specifications of water quality and the maximum speed of water flow. As long as most accelerator laboratories use demineralized water, only a few materials must be considered. Materials suitable for these cooling circuits are stainless steel, copper, tin-free cast bronze, lead-free solder, ceramics and some plastics. This has to be specified!

### 10.3 TRANSMISSION LINE AND CIRCULATOR

There are only two practical choices of the transmission line for transmitting high power; either a coaxial line or a rectangular waveguide.

A waveguide transmission line acts as a high-pass filter and can handle hundreds of kilowatts: The lower the frequency cutoff, the larger the waveguide. All power losses are on the outside wall of the waveguide because there is no inner conductor. When the transmission line is used in megawatt applications, it is filled with pressurized insulation gas. The advantage of a waveguide is its power capacity, but the disadvantages are its large size and low flexibility, making it difficult to mount, especially through the labyrinth of the accelerator's radiation shielding.

Coaxial transmission lines can consist of fixed aluminum- or copper-tubes, or as a flexible line made from corrugated tubes. A coaxial line can be used from DC to an upper frequency limit, where waveguide modes can propagate. In Equ. 10.6, we calculated the cutoff frequency,  $f_c$  (in Hertz), using the diameter of the inner conductor (in mm) of the coaxial line,  $d$ , the inner diameter of the outer conductor,  $D$ , the velocity of light,  $c = 3 \times 10^{11} \text{ mm s}^{-1}$ , and the relative dielectric constant of the material located between the two conductors,  $\epsilon_r$ .

$$f_c = \frac{2c}{\pi\sqrt{\epsilon_r}} * \frac{1}{D + d} \quad (10.6)$$

This limit differs slightly for straight lines and other devices, like bending elbows. Detailed data should be obtained from the manufacturer. About  $\frac{2}{3}$  of the power dissipation is in the inner conductor and  $\frac{1}{3}$  in the outer conductor. This causes stronger heating of the inner conductor than the outer one, which additionally is cooled by the surrounding air. Therefore, at high power levels, they have different temperatures, which lead to two different thermal expansions for the two conductors. For long straight lines, length-compensation is needed. In flexible coaxial lines, this can cause reflections in bends wherein the heated inner conductor with a larger bending radius is pressed out of the center of the line, disturbing the impedance of the transmission line. Hence, there is a dimension and power limit of the coaxial line at about  $80 \text{ kW}_{\text{CW}}$  at 500 MHz, for instance, with a 6 and  $\frac{1}{8}$  inch line, or  $9 \text{ kW}_{\text{CW}}$  at 1.3 GHz with a 3 inch line. The power limit can be shifted by letting air flow between the inner and outer conductor, resulting in convection cooling of the inner conductor. The main advantage of coaxial lines is that they are easy to handle, especially flexible ones. Furthermore, since they are smaller than waveguides, they can be installed easily even if the radiation-protection labyrinths are tight.

Cavities in accelerator applications are operated under high and varying reflection conditions. This will cause problems due to standing waves in the output resonator of the electron tube or in the transistors in a solid-state transmitter. Three-port circulators can protect the RF power source from reflections of the cavity. Using ferromagnetic resonance, they divert the RF power into a matched load. Power fed into port 1 always comes out of port 2; power fed back into port 2 is directed to the matched load on port 3.

## 10.4 RF FUNDAMENTAL POWER-COUPLERS

A fundamental input power-coupler (FPC) is the device that transfers the RF power from the waveguide into the cavity. It matches the generator's output to the impedance of the cavity-beam system that varies from matched impedance to full reflection, depending on the beam's intensity. There are numerous technical requirements. It also must provide a vacuum barrier between the cavity's vacuum and the feeding RF transmission line. In addition, it must meet the cleanliness conditions required for superconducting injector cavities. On the mechanical side, the coupler must cover the thermal shrinkage during cool-down in SC systems and maintain a low static heat-load and minimize mechanical stress on the ceramic windows. Some couplers also have to allow some mechanical flexibility for variable coupling strengths to control the external  $Q$  value.

Since the energy of the beam in injector cavities is quite low and photoinjectors are used to generate low emittance beams, special attention has to be paid to the wakefield kicks produced by the FPC.

When choosing the design of the FPC, the main parameters to consider are the following:

- power level, peak/average
- pulsed/CW operation mode
- RF frequency
- adjustability of coupling strength, if needed
- mechanical boundary conditions
- cooling
- heat leakage (for SC injector cavities)
- sensitivity to multipacting
- coupler kicks on the beam

Several reviews on couplers have been published [10.23]–[10.26]. Three different design principles are of interest for injector cavities. For each approach, we discuss their advantages and difficulties, and give examples. For adapting an injector cavity, detailed calculations have to be undertaken to predict its electromagnetic-, mechanical-, thermal- and multipacting-properties. Before becoming operational, all couplers must be carefully conditioned.

#### 10.4.1 Waveguide Couplers

A simple concept underlies waveguide couplers: A rectangular waveguide with a ceramic window is connected to the cavity cell in a normal conducting cavity, or to the beam pipe close to the cavity cell in superconducting cavities [10.27]. Usually, coupling strength is fixed and depends on the position of the waveguide with respect to the coupling cavity cell and the size and shape of the coupling iris. Coupling can be adjusted over  $\sim 1$  order-of-magnitude, using an external 3-stub waveguide tuner in the waveguide transmission line [10.28]. A waveguide coupler needs more space than a coaxial one, but cooling the former is easier. Cooling is from the outside only, since there is no inner conductor. There is considerable heat leakage of waveguide couplers in superconducting cavities due to the waveguide's size; good thermal anchoring is essential.

Special attention must be paid to the ceramic window that serves as a vacuum barrier between the cavity that is under vacuum and the waveguide that is under air or insulation gas. The soldered joint between the waveguide and the ceramics of the window must be designed very carefully because of the different thermal expansion coefficients of ceramics and the waveguide's metal. Cooling is achieved by attaching copper braids or cooling channels to the wall of the waveguide, or by blowing air onto the ceramics in case of a warm window. Figure 10.12 shows a waveguide coupler tested up to  $800 \text{ kW}_{\text{CW}}$  at a frequency of 700 MHz [10.29]. Most such windows are made of  $\text{Al}_2\text{O}_3$  ceramic that exhibits a high secondary electron emission coefficient. To reduce multipacting, coating it with a thin layer (a few nanometers) of Ti or TiN is essential. Designing the system's geometry without a direct line of sight to the accelerated beam also prevents multipacting [10.30].

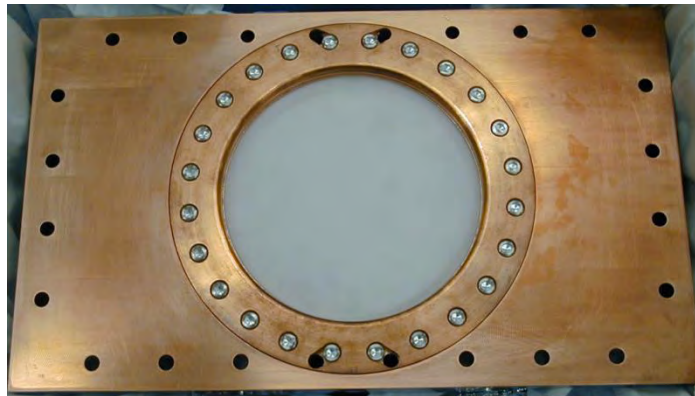


Figure 10.12. Waveguide window tested up to  $800 \text{ kW}_{\text{CW}}$  at 700 MHz. [[10.29]; Available under Creative Common Attribution 3.0 License ([www.creativecommons.org/licenses/by/3.0/us/](http://www.creativecommons.org/licenses/by/3.0/us/)) at [www.JACoW.org](http://www.JACoW.org).]

#### 10.4.2 Coaxial Couplers

Coaxial couplers are more compact than waveguide couplers. In NC cavities, inductive coupling with a coupling loop is popular. SC systems use capacitive coupling *via* the inner conductor, which protrudes into the beam pipe, close to the cavity. These techniques support adjustable coupling factors by turning the loop or changing the penetration depth of the coupler finger. Cooling is more complicated because about  $\frac{2}{3}$  of the losses are dissipated in the inner conductor. Water- or air-cooling can be applied for warm inner conductors.

Figure 10.13(a) is a cross section of the variable coupling, coaxial coupler, developed by Cornell, for use at 1.3 GHz SC cavities; 61 kW<sub>CW</sub> capability was demonstrated [10.31]. It is based on the TTF3 coupler [10.32] developed by Deutsches Elektronen Synchrotron (DESY) (2-3 kW<sub>CW</sub>) and the BESSY coupler (10 kW<sub>CW</sub>) [10.33] developed by HZB. The difference between them is the strength of cooling. In pulsed operation at FLASH, the average power of the TTF3 coupler is low. To use them in CW operated systems, heating of the bellows is the power limiting issue. HZB modified the coupler by introducing a gas-cooling system for the inner conductor. We note that the heat conductivity of the window ceramics has a maximum close to the temperature of liquid nitrogen (and is higher than the temperature coefficient of copper), so the cold inner conductor is cooled *via* the ceramics at the liquid nitrogen intercept. To reduce the coupler kick, the tip of the antenna has the same contour as the beam pipe.

Power capacity can be increased by using fixed coupling without avoiding bellows at the inner conductor of the coupler. Figure 10.13(b) shows a fixed coupling FPC at 1.3 GHz developed for the Koh Ene Ken (KEK) ERL project (Japanese National Laboratory for High-Energy Physics). In the first tests, it demonstrated 100 kW<sub>CW</sub> and 130 kW in pulsed operation, limited by the test environment [10.34]. A higher power capability is expected. It is a scaled version of the KEKB coupler, which has demonstrated 370 kW<sub>CW</sub> at 508 MHz [10.35]. KEKB is the B-meson factory at KEK.

### 10.4.3 Coaxial Waveguide Couplers

Figure 10.14 illustrates the combination of both coupler principles [10.7]. A waveguide to coax transition is realized by using the beam pipe following the gun cavity as the outer conductor of the coaxial line. The electron beam and the laser light pass through the coupler inside the inner conductor of the coaxial line. By this mode of construction, the coupling of the RF power to the cavity is highly symmetrical and the coupler kicks to the beam are small. The disadvantage of this principle is the longitudinal length and the difficulty in implementing HOM dampers.

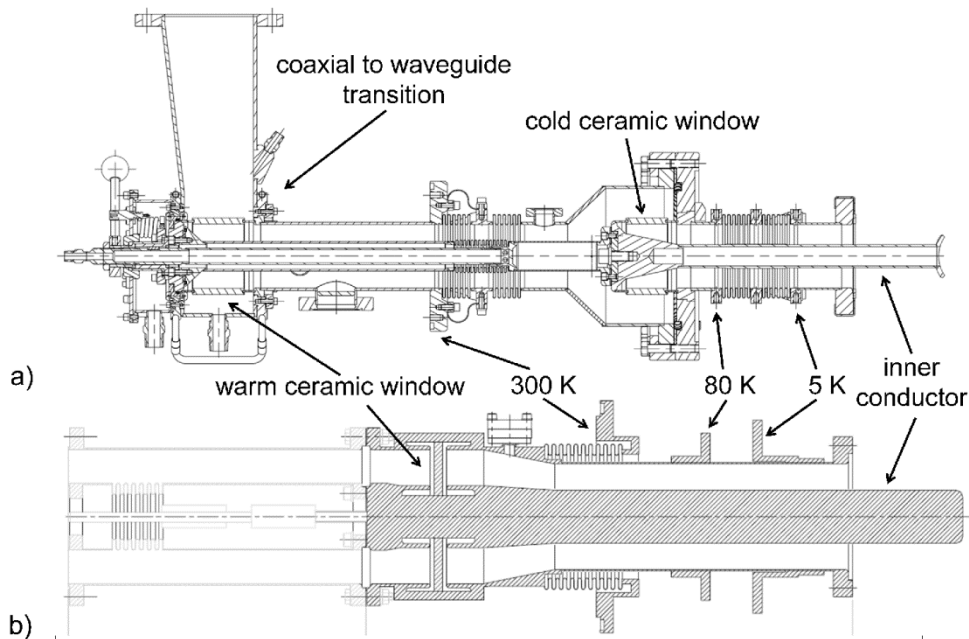


Figure 10.13. Coaxial fundamental power couplers with thermal intercepts at 5 K, 80 K and 300 K. (a) Variable coupler, developed by Cornell, with a demonstrated power capability of 61 kW<sub>CW</sub> at 1.3 GHz using cylindrical windows. (b) Fixed coupling FPC by KEK using a ceramic disc as window. First tests demonstrated 100 kW<sub>CW</sub> at 1.3 GHz but higher values are expected. [[10.31]; Adapted under Creative Common Attribution 3.0 License ([www.creativecommons.org/licenses/by/3.0/us/](http://www.creativecommons.org/licenses/by/3.0/us/)) at [www.JACoW.org](http://www.JACoW.org).]

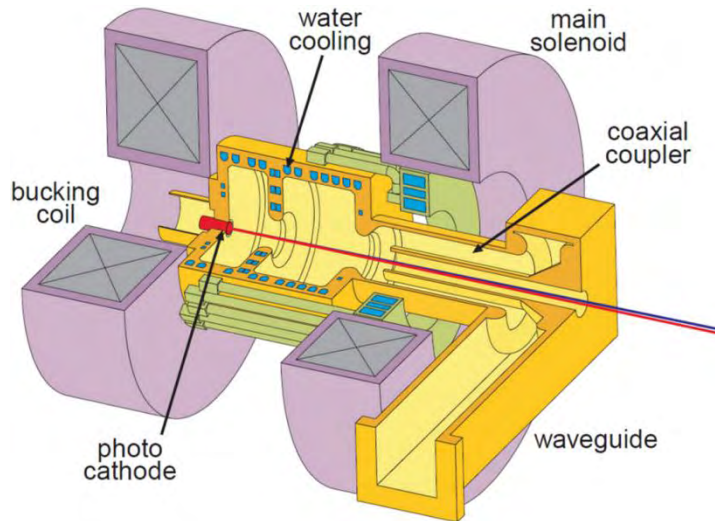


Figure 10.14. Coaxial waveguide coupler as used at PITZ (Photoinjector Test Facility Zeuthen), and at TTF (TESLA Test Facility with TESLA, the Tera Electron Volt Energy Superconducting Linear Accelerator) at DESY. A waveguide to coaxial transition is realized by using the beam pipe as the outer conductor of the coaxial line. The electron beam and the laser light pass through inside of the inner conductor of the coaxial line. This coupler has a high degree of symmetry and the coupler kicks to the beam are small. [Courtesy of K. Flöttmann]

## 10.5 HIGHER ORDER MODE COUPLERS

An accelerating cavity is designed to resonate in the fundamental  $TM_{010}$  mode, but a wide spectrum of other modes also can be excited. The frequencies of these modes are higher than that of the fundamental mode, so they are called higher order modes (HOMs). When the beam passes through the cavity and a frequency component of the beam spectrum has a frequency close to that of the HOM mode, it can excite the HOM. Depending on the  $Q$ -value of the HOM, energy stored in this mode can revert back to the beam, causing longitudinal- and transverse-instabilities that degrade its emittance and broaden its energy. The strength of the HOM is given by its shunt impedance,  $R$ , and its quality factor,  $Q$ ; both values must be kept small.

Monopole modes can cause longitudinal instabilities in the beam and increase its energy spread; dipole-, quadrupole- and sextupole-modes can lead to transverse instabilities. Monopole and dipole modes inflict the highest impedance. Thus, when designing the damper, the modes' different polarizations have to be account for.

We mention that care must be taken so only the HOMs are damped and the fundamental accelerating mode left unaffected; hence, rejection filters or other filtering techniques are essential.

An overview on HOM damping techniques is given in [10.26], [10.36]. There are three design principles for injector cavities of interest: Waveguide couplers; coaxial couplers; and, beam pipe couplers. We discuss and illustrate an example of each of these types.

### 10.5.1 Waveguide HOM Couplers

A waveguide is a frequency high-pass device, simplifying rejection of the fundamental mode. The cut-off frequency is set such that the lowest HOM can propagate in the guide, but the fundamental mode is rejected. More than one damper is required because dipole modes have two polarizations. Detailed calculations are necessary to ensure that all HOM modes can propagate to the dampers and no modes are trapped in the cavity. For NC cavities, the HOM dampers are attached directly at the cavity cell: for SC cavities, they are placed at the beam pipe close to the cavity. Figure 10.15 shows a cavity using six waveguide HOM couplers

on a five-cell SC cavity [10.37]. The terminating loads are at room temperature. The waveguide dampers are transversal space consuming devices, but their longitudinal space requirement is low.

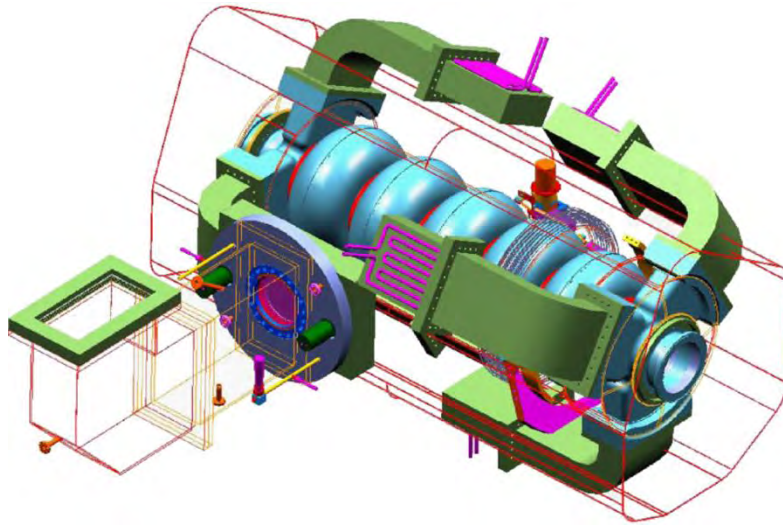


**Figure 10.15.** Six waveguide HOM couplers are attached to a five-cell SC cavity developed by JLab (Jefferson Laboratory) to ensure heavy damping of all polarizations of modes. The terminating loads are at room temperature. [[10.37]; Available under Creative Commons Attribution 3.0 License ([www.creativecommons.org/licenses/by/3.0/us/](http://www.creativecommons.org/licenses/by/3.0/us/)) at [www.JACoW.org](http://www.JACoW.org).]

Above the cut-off of the waveguide, all coupled modes from the cavity can propagate to the load. The terminating loads at the end of the waveguide can be used at room temperature even in SC cavities. Ferrite loads may be applied in vacuum when using special materials with low outgassing rates. In separating the cavity's vacuum and the load with a window, we need to remember that most ceramics have limited transmission characteristics at the very high frequencies such as those contained in the HOM spectrum of an injector for short electron bunches.

The absorbing waveguide load is separated from the cavity and can be maintained at room temperature even in SC cavities making the waveguide couplers a good choice in applications with very high HOM power loads. Flanges and windows should be placed far enough from the cavity to ensure that the power level of the fundamental mode of the cavity is low at both.

### 10.5.2 Coaxial HOM Couplers

A coaxial HOM coupler consists of an inductive coupled pick-up loop, or a capacitive coupled antenna to transfer the energy of the HOMs from the cavity. These antennas might be resonant fingers for damping single modes, or broadband matched couplers, feeding the HOM power to an external load *via* cable. In all cases, it is essential to reject the fundamental frequency using a filtering unit, which makes their design more difficult. This rejection filter must be carefully tuned, typically to rejection values of -70 dB or better. The HOM dampers are attached directly at the cavity cell in NC cavities, or at the beam pipe close to the cavity for SC cavities.

Figure 10.16 illustrates the HOM coupler with double fundamental-mode rejection filter used at KEK [10.38]; it is a development of the TESLA-type HOM coupler [10.39] having a single rejection filter. An antenna in the beam tube close to the cavity picks up the HOM energy. The geometry of the pickup loop results in a rejection filter for the cavity's fundamental frequency. The filter frequency is tuned by changing (deforming) the distance from the far end stub to the HOM filter housing. The HOM energy is coupled with a feedthrough into a cable. The TESLA HOM coupler is cooled solely by the heat conduction of the

niobium beam pipe. For higher CW applications, this type of cooling is insufficient so that the inner conductor warms up and eventually quenches, causing Q-switches in the cavity. CW operation is made possible by using sapphire as an insulating material [10.40]; its high thermal conductivity leads to better cooling of the inner conductor.

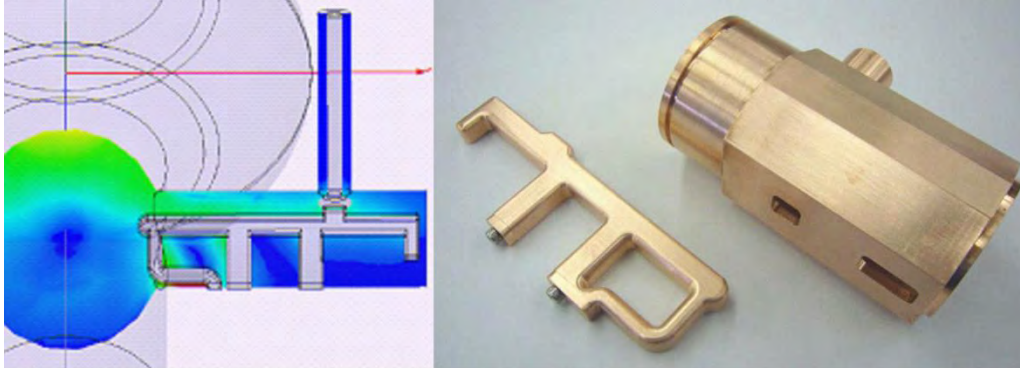


Figure 10.16. Coaxial HOM couplers developed by KEK that employ a double notch filter to increase the rejection of the accelerating mode of the cavity. The colors in the left picture symbolize the magnetic field strength. [[10.38]; Available under Creative Commons Attribution 3.0 License ([www.creativecommons.org/licenses/by/3.0/us/](http://www.creativecommons.org/licenses/by/3.0/us/)) at [www.JACoW.org](http://www.JACoW.org).]

Coaxial HOM couplers need to match the required frequency characteristics to fulfill multipacting restrictions and to account for boundary conditions by power limitations. This means that extensive electromagnetic- and thermal-calculations are a prerequisite. We note that the ceramics or sapphires at the feed through have restricted transmission characteristics at very high frequencies. The frequency limitation of sapphire is at about 6 GHz! The space consumption of a coaxial HOM coupler is low. Its power capability mostly is limited by the feed through, attached cable and the cooling applied.

### 10.5.3 Beam Pipe HOM Couplers

Beam pipe HOM couplers afford another option for superconducting cavities. The beam pipe opening at a SC cavity is large enough to act as a waveguide above cutoff for HOM frequencies while rejecting the fundamental mode. The beam pipe houses high power ferrite loads at liquid nitrogen- or room-temperature to damp the propagation. Due to the fact that the beam pipe is acting as a waveguide to the HOM, the cutoff of the beam pipe has to be low such that all HOM modes can propagate to the absorbers. It is important to ensure that the dipole modes at lower frequencies can propagate into the beam pipe. Because the beam pipe opening of NC cavities is small and thereby the cutoff is high, beam pipe HOM absorbers are not applicable for NC cavities.

Using different ferrite materials achieves smooth damping characteristics over a wide frequency range. Figure 10.17(a) [10.41] shows a beam pipe ferrite absorber developed at Cornell University. Three different ferrite materials are used to give overall good damping characteristics up to 40 GHz.

The power dissipation capability of beam pipe absorbers depends highly upon the mass of ferrite used. The drawback of beam pipe absorbers is their longitudinal space consumption, *viz.* lowering the filling factor of modules. A second problem occurs when cooling the ferrites to the temperature of liquid nitrogen to reduce static losses in SC systems; the conductivity of ferrites drops, resulting in electrostatic charging by the passing beam, discharges and strong kicks to the beam. So far, there is no solution, although research is underway. Figure 10.17(b) and Figure 10.17(c) show a ferrite ring operated in the FLASH accelerator [10.42]. The designed power capability is 100 W and frequency ranges up to tens of gigahertz.

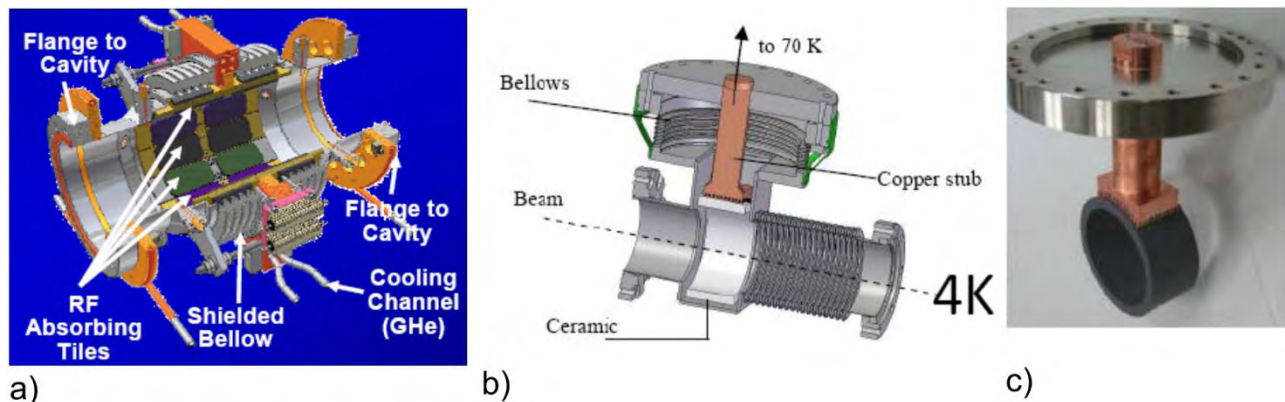


Figure 10.17. Beam pipe HOM coupler using ferrites and ceramics. (a): Three different materials are used to cover a wide frequency range. (b) and (c): A ceramic ring adapted to the beam pipe diameter. [[10.41]; Adapted under Creative Common Attribution 3.0 License ([www.creativecommons.org/licenses/by/3.0/us/](http://www.creativecommons.org/licenses/by/3.0/us/)) at [www.JACoW.org](http://www.JACoW.org).] [[10.42]; Available under Creative Common Attribution 3.0 License ([www.creativecommons.org/licenses/by/3.0/us/](http://www.creativecommons.org/licenses/by/3.0/us/)) at [www.JACoW.org](http://www.JACoW.org).] [[10.42]; Adapted under Creative Common Attribution 3.0 License ([www.creativecommons.org/licenses/by/3.0/us/](http://www.creativecommons.org/licenses/by/3.0/us/)) at [www.JACoW.org](http://www.JACoW.org).]

## 10.6 LOW-LEVEL RF CONTROL FOR PHOTOINJECTOR RF CAVITIES

In very general terms, the major task of the LLRF is to maintain a constant energy gain of the beam in the accelerating cavities. This is achieved by measuring the field level of the accelerating mode in the cavity at a given phase of the bunched beam with respect to the field and determine the deviation of that value to a given reference value. Finally, we must assure the compensation of that deviation by altering the low power signal that drives the RF power amplifier.

There are four major types of application:

1. Normal conducting cavities, *e.g.* made from copper, for high power RF operation at low duty factor, pulsed mode to accelerate a beam organized in bunch trains, as in the X-FEL project [10.6]
2. Normal conducting cavities at low- to intermediate-field levels at high duty factor for high current application [10.43]
3. Superconducting cavities for low beam current CW operation, *e.g.* the ELBE FEL [10.43]
4. Superconducting cavities for high beam current CW operation being developed for future ERL projects [10.44]

Two major questions drive the design of the LLRF system: First, what is the needed amplitude and phase stability of the field compared with the reference? This query leads to the issue of the required accuracy with which the field vector is to be sampled and processed. Second, what is the bandwidth of the system to be controlled? Is it more a broadband NC cavity driven in pulsed mode, where the pulse's ramping time and flat-top properties have to be controlled properly; or, does it pertain to handling a bandwidth in the Hertz regime, such as the ones in low beam current, CW driven, superconducting cavity?

Often, it is useful to start designing the LLRF system by analyzing the possible sources of errors that detune the cavity and entail deviations of the field vector from the reference. This is accompanied by properly evaluating the RF reference system that determines the noise of the LLRF and the jitter and drift between the major components driving the photoinjector, *viz.*, the laser system and the controlled accelerating field. A helpful tool for setting the boundary conditions for stable operation within requirements is to mathematically simulate the RF cavity and the feedback system, including the known or modeled error sources [10.45].

Keeping the power requirements (Equ. 10.4) in mind, we summarize the following error sources for field stability of RF cavities:

### **NC Cavity:**

- In comparison to a SC cavity, NC cavities have low intrinsic quality factor of  $Q_0 \approx 10^4$  due to their high surface resistance. For an L-band cavity, this corresponds to a natural bandwidth of several kilohertz. Nevertheless, due to the high ohmic-wall losses, the cavity must be cooled and any shift in temperature detunes it. Values of 23 kHz per degree Celsius were measured for a NC one-and-a-half-cell photoinjector cavity [10.46].
- In high power pulsed operation, overshoots and oscillations may occur that must be compensated by fine tuning the feedback parameters.

### **SC Cavity, Low Beam Loading, High Power Pulsed Mode:**

- The components of the electric- and magnetic-fields of the standing RF wave interact with the currents in the cavity wall, exerting a net force on the cavity wall, the so-called Lorentz force detuning [10.47]. Usually, detuning is about  $1\text{-}3 \text{ Hz m}^2 \text{ MV}^{-2}$ , that detunes a cavity operating at  $35 \text{ MV m}^{-1}$  by more than a kilohertz. In the pulsed mode, this is comparable to a step response of the mechanical cavity system. Thus, over the length of the pulse, decaying mechanical eigenmodes alter the field level; an effect which can only partly be compensated by tuning systems [10.48].

### **SC Cavity, Low Beam Loading, CW Operation:**

- The external quality factors of cavities operated at CW, with low beam loading, are optimized to cope with the external mechanical cavity-detuning. In CW operation, microphonic detuning is the major source of errors in field stability. Mechanical oscillations from the vacuum pump and the liquid helium supply are coupled *via* beam pipes or the helium vessel to the cavity's mechanical eigenmodes. Even a nanometer deformation shifts the frequency by 0.3 Hz [10.1].
- The thin-walled niobium cavities are very susceptible to variations in helium pressure. Detunings of  $1.46 \text{ Hz Pa}^{-1}$  due to pressure dependencies were measured [10.49]. Fast piezo-based tuning schemes and passive stiffening systems are needed to minimize this source of error.
- Even in the CW mode, the Lorentz force detuning may create instabilities. Residual field fluctuations from strong microphonics cause further detuning due to the Lorentz forces. If there is insufficient power in the control loop, the cavity field may trip, the so-called ponderomotive instability that appears in generator driven loops [10.50], [10.51].

### **Beam Related Effects:**

- An electron bunch passing through the cavity extracts energy from the field proportional to its charge as a function of the RF phase. This can be measured as a transient in the field's amplitude. Due to shot-to-shot variations in laser intensity, charge fluctuates, leading to a linear increase of the beam's energy spread with that fluctuation. This effect depends on the field decay time constant, the gain of the RF feedback loop and the bunch's repetition rate.
- Time jitter of the laser with respect to the reference and phase errors of the controlled RF field might produce an increase of the beam's energy spread after the injector's cavity. Even for electron beams that are not fully relativistic, RF phase dependent velocity bunching occurs that may increase the timing jitter of the beam in the drift sections after the injector.

### RF Control Related Effects:

- The measurement of the cavity field at the pick-up probe, or *via* the reflected power signal, may be falsified by measurement noise, drifts, noise in the RF cabling and nonlinearities in the RF mixers.
- The total noise of a system limits its performance. During high gain operation, amplified noise creates a gain dependent increase in field errors; hence, noise limits field control through the gain of the system. Thus, in addition to using low noise hardware throughout the entire reference system, including all oscillators and the clock generation for the LLRF, must be optimized for low phase noise.
- In RF amplifiers, the gain and phase response of the output wave alter as a function of the driving input signal. This effect is predictable, and thus can be compensated by using feedforward tables, or an additional feedback loop [10.52].
- Fast fluctuations of the power supply, *e.g.* the klystron cathode, causes a ripple in the output power due to velocity effects of the beam in the klystron's cavity and drift sections. Effectively, this acts as phase noise modulation on the forward power. Compensation is achieved by measuring the klystron ripple and implementing an additional feedback loop [10.53].
- Noise in the RF feedback loop may excite unwanted modes of the cavity pass-band, as was reported for TESLA cavities [10.54] during vertical acceptance tests, and also during LLRF operation at a horizontal test stand at HZB. This issue depends on the phase of the other pass-band modes with reference to the  $\pi$ -mode in the cell where the field is measured with a pick-up antenna. Furthermore, the total time delay of the feedback loop, together with that phase dependence, sets the boundary for stable operation [10.55].

Mathematically, all these effects are summarized in the following formulas.  $E_{kin}$ , the energy gained by the particle bunch, is a function of the experienced accelerating field  $E_{acc}$  given by its current longitudinal position,  $z$ , and the elapsed time  $t$  since its extraction from the photocathode,

$$E_{acc}(t,z) = [E_z(z) (1 + \sigma_A)] \cos\left(\Phi_b + \sqrt{\sigma_{\Phi_{inj}}^2 + \sigma_\phi + \omega t}\right) \quad (10.7)$$

$$E_{kin}(t,z) = e \int E_{acc}(t, z) dz \quad (10.8)$$

with  $\Phi_b$  the injection phase with respect to the RF field with frequency  $\omega$ , the phase error due to the laser jitter,  $\sigma_{\Phi_{inj}}$ , and the phase- and relative-amplitude errors of the RF field,  $\sigma_\phi$  and  $\sigma_A$ , respectively.  $e$  is the particle's charge. The LLRF system needs to resolve these field errors and compensate for them by altering the forward wave coupled to the cavity. Time jitter of the laser system at least can be minimized by assuring proper synchronization between the RF and laser system.

#### 10.6.1 RF Control Strategies: Field and Tuning Control

Modern field control systems implement a huge variety of functions to operate, control and survey a cavity. To allow for flexible implementation of filters, feedback- and feedforward- algorithms, and rather complex codes to cope with the complex mechanical cavity transfer function; nowadays, most LLRF systems are built on digital hardware. Analog systems still are in operation and often special fast loops, *e.g.* for klystron control, are sometimes implemented as an analog circuit. However, with the availability of fast ADC converters with a more than 14-bit resolution, most modern systems rely on digital implementation. It is easier to incorporate the LLRF system in the accelerator's control system, supporting well correlated measurements between the beam's properties and the stability of the LLRF cavity.

Furthermore, digital hardware is easy to configure with several modes of operation, remotely controllable and eases changing of the system's parameters without needing to exchange hardware components.

Nowadays, there are a huge variety of digital LLRF systems operating worldwide [10.52], [10.53], [10.56]–[10.58]. Mostly, they were developed for operation of main linac- or storage ring-cavities, even allowing the vector sum control of up to eight cavities [10.59]; they were not specifically designed to operate photoinjector cavities. Nevertheless, due to their intrinsic flexibility, it is easy to adapt them to controlling the injector. Depending on the personnel available at a laboratory, the choice is between commercial systems based on Digital Signal Processing (DSP) boards [10.56], [10.60], or custom design, based on their own hardware solutions (*e.g.* [10.53]).

The LLRF feedback loop itself mostly is implemented as a standard Proportional-Integral (PI) controller, as described in any control theory textbook (*e.g.* [10.61]) and is a rather simple algorithm. For good performance, it must be fast, with a high resolution better than 14 bits sampling ADCs. This is essential to achieve a small group delay, below a microsecond or even several hundred nanoseconds. A high sampling rate is mandatory for a small phase lag of the loop to allow a high gain margin. High-bit resolution is required to resolve small field deviations, so supporting control in the  $< 1/1000$  regime. Also, the system should enable a fast change of control parameter during operation and a deterministic handling of the processed signals, the prerequisite for a numerical stable time-discrete system.

A Field Programmable Gate Array (FPGA) chip can meet all these features [10.62]. The core feedback functions of nearly all modern LLRF systems are performed by an FPGA-based digital system. It directly accesses the sampled signals of the fast ADCs and often features some SRAM memory blocks to load different algorithms to the FPGA or supports the transfer of parameters and data. For general operability, the FPGA is embedded into some general DSP system that houses control loops operating on a slower time scale (as cavity tuning), the communication to the accelerator control system (*e.g.* EPICS [10.63]), a state machine or similar to monitor the cavity state.

In the following subsection, the set-up and functioning of a digital LLRF system is explained in the context of a generic system.

### 10.6.2 A Generic System

An LLRF field control system has two major components: the analog RF hardware consisting of RF mixers, vector modulators, low-pass and band-pass filters, and small amplifiers. The digital hardware including the fast ADCs and DACs, onboard memory, slow ADCs/DACs, and FPGA, plus DSP chips for the signal processing and controller implementation. Furthermore, there may be auxiliary hardware to record fast interlock events, amplifiers for piezo tuners and stepping motor control for driving mechanical cavity tuner or plunger tuner.

The analog RF hardware has the major task of providing the control loop with low power signals of all measurable power signals describing the state of a cavity. These are the forward power provided by the high power amplifier to the cavity *via* the fundamental power coupler, the power reflected at the cavity due to (wanted) impedance mismatch, and finally, the transmitted power to measure the field vector. As L-band cavities operate at 1.3 GHz, several gigahertz ADCs with 14-bit resolution are needed to measure the field. The analog RF hardware thus is often referred to as the down-converter. It transforms the cavity frequency by mixing it with a reference to a measurable intermediate frequency (IF) that still contains the amplitude and phase information of the accelerating mode. This is a valid procedure, as all error sources changing the

cavity field happen on a slower timescale than the cavity frequency; the LLRF system, therefore, measures the envelope of the field. Lower frequency structures (some hundred megahertz) are controlled by directly sampling the field vector.

### 10.6.2.1 Principle of Field Detection

The amplitude and phase of the field often is measured by sampling the real- and imaginary-components of the RF signal by the intermediate step of down-conversion to a lower frequency. This method often is termed IQ demodulation, quadrature demodulation, or complex demodulation. I and Q represent the “In-Phase” and “In-Quadrature,” respectively, and are the complex representation of the RF signal. To reconstruct the signals’ content in accordance with the Nyquist criterion, it should be sampled at twice the rate of the highest frequency component. Therefore, the cavity pick-up signal is down-converted to an IF, still containing the side-band information of the cavity’s field variations.

The demodulation contains three steps:

- down-conversion or down-mixing by an RF mixer circuit
- low-pass filtering to remove the higher frequency content of the mixing process resulting in the IF
- IQ sampling of the IF, e.g. by oversampling to resolve the field’s I and Q components

Figure 10.18 shows the principle of the IQ detection by oversampling of the RF signal four times. The sinusoidal IF signal is sampled every  $\pi/2$  in the unity circle representation. A measurement of the real amplitude at that time gives, as a consecutive data stream, the components I, Q, -I, -Q, I, and so on. As the sampling starts randomly at some phase, the feedback loop itself is a phase delay and all IQ components have to be shifted to the first quadrant of the unity circle; also, the IQ components are rotated in phase by a two-by-two rotation matrix to supply the digital control algorithm with the real- and imaginary-field components.

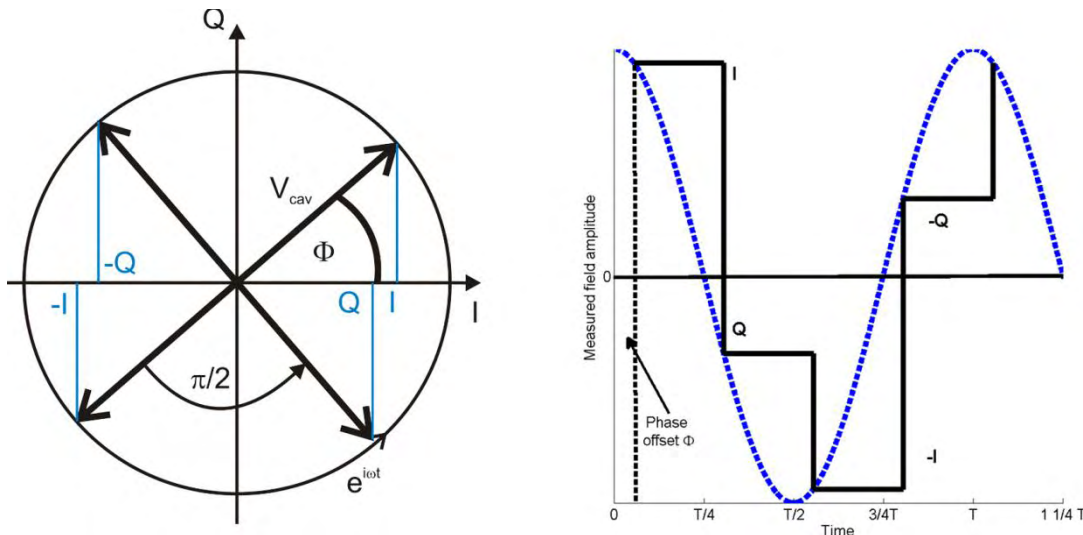


**Figure 10.18.** Principle of detecting the field vector component (IQ detection) by four times oversampling of the IF signal following down-conversion. Each consecutive sample is shifted by  $\pi/2$  in phase, thus representing the In-Phase and In-Quadrature component of the field. Every two samples thus deliver information to reconstruct the field vector. The measurement starts to sample field components at an arbitrary phase offset  $\Phi_0$ , which has to be corrected for by determining the loop’s phase shift.

After the signal is processed by the feedback in the FPGA, there are two ways to reconstruct the phase and amplitude corrected output signal to the cavity: the IQ components are fed *via* two individual DACs to a

vector modulator varying the forward power-wave; or, the IQ components internally modulate a digital up-converter, similar to a vector modulator, and the output IF after the DAC is mixed with the shifted LO signal to the 1.3 GHz forward-power signal.

### 10.6.2.2 An Example

Figure 10.19 shows a generic field control system for a photoinjector RF cavity. The RF reference and clock system supplies all analog signals to operate the cavity and LLRF system: these are the RF cavity's fundamental mode; a frequency, shifted by the IF frequency, for mixing the three power signals of the cavity down to the IF; the sampling clock frequency of the ADCs (often four times the IF); and, the reference frequency to lock the laser to the cavity RF. For example, assuming a cavity operating at 1.3 GHz, the reference system would provide a 1.3 GHz signal twice, at least three 1.28 GHz signals for an IF of 20 MHz, and a clock signal of 80 MHz.

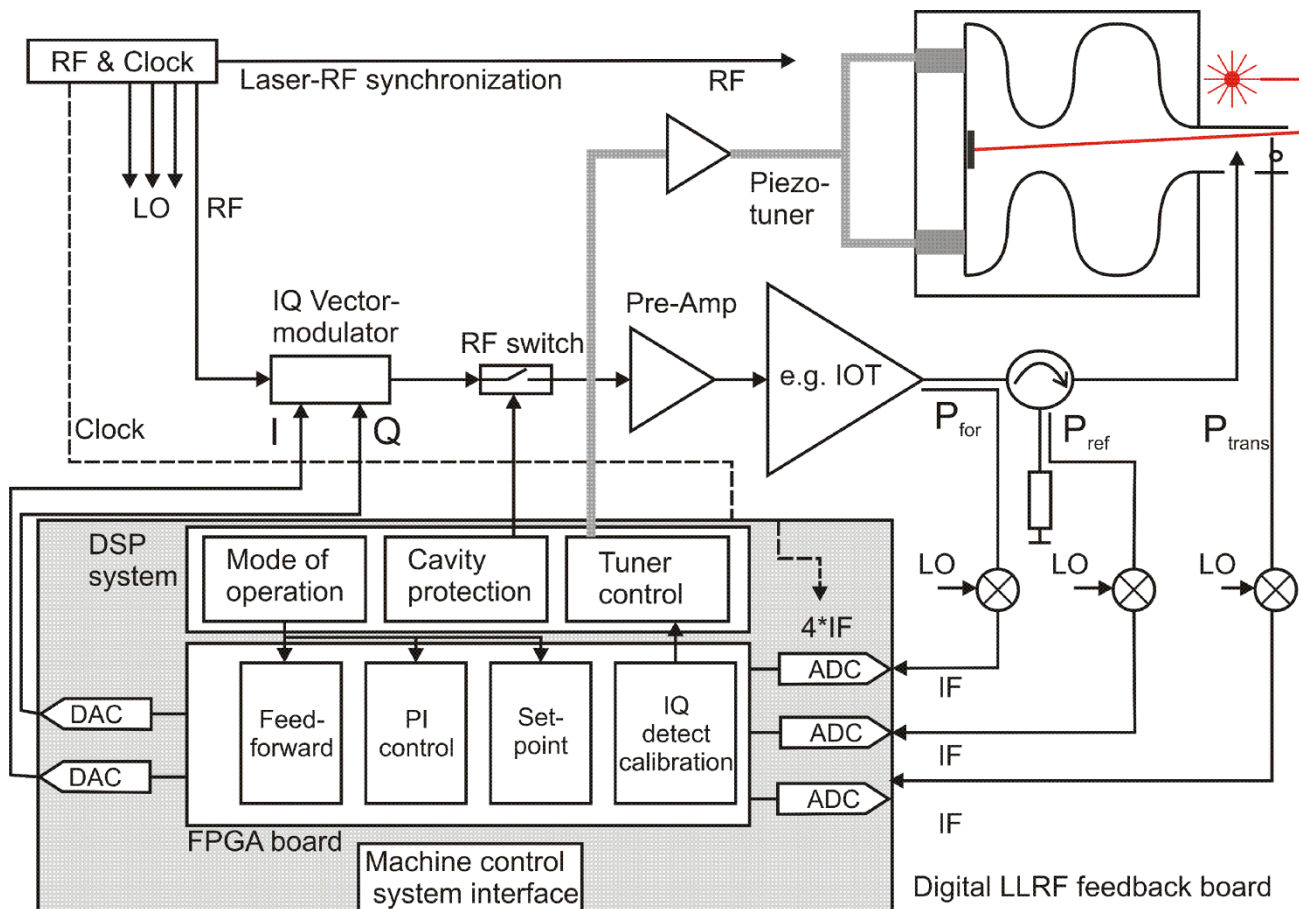


Figure 10.19. Layout of a generic digital single-cavity RF control system in a generator-driven set-up. It incorporates a fast field programmable-gate array, a digital signal processing unit to detect cavity RF interlock events, fast- and slow- tuning control algorithms and general procedures for different modes of operation. Further, there is an interface to the machine-control system. The reference for the field-control system is the RF and clock generation system that also synchronizes the photoinjector's laser system.

The 1.3 GHz forward signal from the reference system drives the cavity. With a vector modulator, it can be shifted in amplitude and phase by the LLRF system, providing the In-Phase and In-Quadrature components for vector modulation to correct the measured field level. In addition, there is some RF switch, *e.g.*, a pin diode, to switch the forward power during an interlock event. This signal then is amplified *via* a pre-amplifier by the main high power unit, to supply the cavity with the needed forward power. As reflections would destroy the IOT or klystron, a circulator directs the reflected power to a water-cooled load.

The power signals usually are obtained by weakly coupling to the transmission line with a directional coupler. The level of the transmitted power obtained by the pick-up antenna intrinsically is low; only weak coupling is needed to measure the field. These signals are down-converted at RF mixers to the IF. The In-Phase- and In-Quadrature-field components are detected by four times oversampling, thus providing the LLRF system every two sampling steps with the full field vector, or amplitude and phase. In this example, the IQ pair of values would be updated at a rate of a 40 MHz. Depending on the bunch's repetition rate, a much lower data rate often is sufficient for control, such that an initial filtration can be achieved by averaging over 40 samples, for example. To reject the excitation of other modes of the pass-band, the transmitted power IQ signal can be processed by special notch filters at the mode's frequency and, in general, low-pass filtered. The amplitude and phase of the filtered signal is compared to those of the desired set point and the resulting error signal is amplified by the PI control gain settings.

In pulsed operation or repetitive errors, often a feedforward value is added to the amplified control signal. This IQ pair finally is connected to the vector modulator, *via* the DACs, to steer the forward power, thereby to close the feedback loop.

In parallel to the FPGA for LLRF feedback, there may be further DSP systems that contain feedback and feedforward loops for tuning control and receiving the tuning angle of the cavity from the LLRF loop. Furthermore, all kinds of algorithms may be programmed on that DSP system to change automatically loop parameters on the FPGA, or to implement different modes of operation, such as ramping the field in CW-operated cavities by using the tuner.

### 10.6.3 Steps towards an LLRF Control

As this part of the book only can give a short introduction into LLRF control design and operation, the following list offers an overview of how to prepare a LLRF feedback system for operating the cavity.

1. Evaluate the required performance of the LLRF control system by calculating the needed phase and amplitude stability of the cavity's accelerating mode. This is obtained by tolerance studies of particle tracking codes.
2. Consider the frequency of the cavity's fundamental mode and further modes in the pass-band. How close is the next pass-band mode to the accelerating  $\pi$ -mode?
3. Determine the cavity's bandwidth and simulate the error sources that could detune the cavity mode (for CW or pulsed operation) to gain insights to the physics that define boundary conditions for a stable operation.
4. Plan tuning schemes operating parallel to the LLRF feedback loop.
5. Assess the needed loop bandwidth to compensate for detuning effects and beam loading effects; consider the beam's repetition rate.
6. Perform a stability analysis using methods of control theory to determine the attainable margins in gain and phase; especially determine a goal for the loop's group delay, and thus the needed sampling time constant of the time-discrete system.
7. Sketch a field control design including LLRF control, tuner control and necessary interlock events to protect the cavity and modes of operation, which will be useful for photoinjector operation.
8. Appraise the available hardware, whether to buy a fully integrated commercial system or to choose a full in-house development. Especially consider ADC/DAC sampling rates, bit resolution and the number of NAND gates of the FPGA chip.
9. Choose a programming code; *i.e.*, closer to FPGAs, such as VHDL or Verilog, or some higher programming language with the needed translation tools, like MATLAB<sup>TM</sup>.

10. Prepare for the interface between the local LLRF system and the accelerator's control system.
11. Design and build a low-noise plus low-drift RF clock and reference system.
12. Program and test the feedback code supported by LLRF simulations at a low power level using a known dummy cavity. A test using signal sources is useful for first tests.
13. Once these steps are completed, start with low power tests at low cavity field amplitudes to test the full system to identify any further inconsistencies.

## 10.7 CONFLICT OF INTEREST AND ACKNOWLEDGEMENT

We confirm that this article content has no conflicts of interest and would like to acknowledge the support of *Deutsches Bundesministerium für Bildung und Forschung* and *Land Berlin*. We would also like to thank H. Bohlen from CPI, G. Blokesch from PPT, E. Weihreter, H.G. Hoberg, and Jens Knobloch from HZB and Ti Ruan from Soleil for fruitful discussions.

### References

- [10.1] A. Neumann, W. Anders, O. Kugeler *et al.*, "Analysis and active compensation of microphonics in continuous wave narrow-bandwidth superconducting cavities," *Phys. Rev. ST Accel. Beams*, vol. 13, pp. 082001-1–082001-15, August 2010.
- [10.2] E. Buechner, F. Gabriel, E. Grosse *et al.*, "The ELBE-Project at Dresden-Rossendorf," in *Proc. 2000 European Particle Accelerator Conf.*, 2000, pp. 732-734.
- [10.3] M. Abo-Bakr, W. Anders, T. Kamps *et al.*, "BERLinPro - a prototype ERL for future synchrotron light sources," in *Proc. 2009 Superconducting RF Conf.*, 2009, pp. 223-227.
- [10.4] P. Emma, R. Akre, J. Arthur *et al.*, "First lasing and operation of an ångstrom-wavelength free-electron laser," *Nature Photonics*, vol. 4, pp. 641-647, August 2010.
- [10.5] A. Fabris, P. Craievich, P. Delgiusto *et al.*, "Progress of the S-Band RF systems for the FERMI@ELETTRA Linac," in *Proc. 2009 Particle Accelerator Conf.*, 2009, pp. 2039-2041.
- [10.6] M. Altarelli, R. Brinkmann, M. Chergui *et al.*, Eds., *The European X-Ray Free-Electron Laser*, Technical design report, Hamburg: DESY XFEL Project Group, 2006.
- [10.7] B. Dwersteg, K. Flöttmann, J. Sekutowicz *et al.*, "RF gun design for the TESLA VUV free electron laser," *Nucl. Instrum. Meth. A*, vol. 393, pp. 93-95, July 1997.
- [10.8] S. Belomestnykh, Z. Conway, J. Dobbins *et al.*, "CW RF systems of the Cornell ERL injector," in *Proc. 2008 Linear Accelerator Conf.*, 2008, pp. 857-859.
- [10.9] I. Ben-Zvi *et al.*, "The ERL high-energy cooler for RHIC," in *Proc. 2006 European Particle Accelerator Conf.*, 2006, pp. 940-944.
- [10.10] A. V. Haeff, "Electron Discharge Device," U.S. Patent 2,284,733, June 2, 1942.
- [10.11] L. S. Nergaard, "Electron Discharge Device," U.S. Patent 2,329,778, September 21, 1943.
- [10.12] M. Di Giacomo, "Solid state RF amplifiers for accelerator applications," in *Proc. 2009 Particle Accelerator Conf.*, 2009, pp. 757-761.
- [10.13] M. Langlois, J. Jacob and J. M. Mercierl, "Cavity combiners for transistor amplifiers," in *6<sup>th</sup> Workshop CW High Average Power RF*, 2010.
- [10.14] P. Pérez, B. Baricevic, P. Sánchez *et al.*, "High power cavity combiner for RF amplifiers," in *Proc. 2006 European Particle Accelerator Conf.*, 2006, pp. 3215-3217.
- [10.15] H.-G. Hoberg, W. Anders, A. Heugel *et al.*, "Highly stable IOT based 1.3 GHz/16 kW RF power source for CW operated SC Linacs," in *Proc. 14<sup>th</sup> Int. Conf. RF Superconductivity*, 2009, pp. 679-682.
- [10.16] K. Buerkmann, M. Abo-Bakr, W. Anders *et al.*, "Status of the Metrology Light Source," in *Proc. 2006 European Particle Accelerator Conf.*, 2006, pp. 3299-3301.

- [10.17] International Study Group, "International study group progress report on linear collider development," SLAC-Report-559, 2000, Chapter 4.
- [10.18] G. Blokesch, private communication, 2010.
- [10.19] W. Kaesler, "A long-pulse modulator for the TESLA test facility (TTF)," in *Proc. 2004 Int. Linear Accelerator Conf.*, 2004, pp. 459-461.
- [10.20] G. E. Dale, H. C. Kirbie, W. B. Haynes *et al.*, "Design, and application of a diode-directed solid-state marx-modulator," in *Proc. 15<sup>th</sup> Pulsed Power Conf.*, 2005, pp. 1211-1214.
- [10.21] D. Bortis, J. Biela and J. W. Kolar, "Active gate control for current balancing in parallel connected IGBT modules in solid state modulators," in *2007 Pulsed Power Conf.*, 2007, pp. 1323-1326.
- [10.22] Puls-Plasmatechnik GmbH, Feldstraße 56, 44141, Dortmund, Germany.
- [10.23] B. Rusnak, "RF Power and HOM Coupler Tutorial," in *11<sup>th</sup> Int. Workshop RF Superconductivity*, 2003.
- [10.24] S. Belomestnykh, "Overview of input power coupler developments, pulsed and CW," in *Proc. 13<sup>th</sup> Int. Workshop RF Superconductivity*, 2007.
- [10.25] M. Champion, "RF input couplers and windows: Performances, limitations, and recent developments," in *Proc. 1995 Workshop RF Superconductivity*, 1995, pp. 195-221.
- [10.26] H. Padamsee, *RF Superconductivity*, Weinheim: Wiley-VCH Verlag, 2009.
- [10.27] V. Nguyen, H. L. Phillips and J. Preble, "Development of a 50 kW CW L-band rectangular window for Jefferson Lab FEL cryomodule," in *Proc. 1999 Particle Accelerator Conf.*, 1999, pp. 1459-1461.
- [10.28] V. Veshcherevich and S. Belomestnykh, "Correction of the coupling of CESR RF cavities to klystrons using three-post waveguide transformers," LEPP Cornell University, Ithaca, NY, Report SRF020220-02, 2002.
- [10.29] R. Rimmer, E. F. Daly, W. R. Hicks *et al.*, "The JLab ampere-class cryomodule," in *Proc. 2001 Workshop RF Superconductivity*, 2001, pp. 567-570.
- [10.30] J. Preble, "CEBAF energy upgrade program including re-work of CEBAF cavities," in *Proc. 2007 Workshop RF Superconductivity*, 2007, pp. 756-760.
- [10.31] V. Veshcherevich, S. Belomestnykh, P. Quigley *et al.*, "High power tests of input couplers for Cornell ERL injector," in *Proc. 2007 RF Superconductivity*, 2007, pp. 517-519.
- [10.32] W.-D. Möeller for the TESLA Collaboration, "High power coupler for the TESLA test facility," in *Proc. 1999 Workshop RF Superconductivity*, 1999, pp. 577-581.
- [10.33] W. Anders, J. Knobloch, O. Kugeler *et al.*, "CW operation of superconducting TESLA cavities," in *Proc. 2007 Workshop RF Superconductivity*, 2007, pp. 222-226.
- [10.34] S. Noguchi, E. Kako, M. Sato *et al.*, "Present status of superconducting cavity system for CERN injector linac at KEK," in *Proc. 2010 Int. Particle Accelerator Conf.*, 2010, pp. 2944-2946.
- [10.35] H. Nakai, K. Akai, E. Ezura *et al.*, "Status report of superconducting RF activities in KEK," in *Proc. 2001 Workshop RF Superconductivity*, 2001, pp. 76-80.
- [10.36] J. Sekutovicz, "HOM damping and power extraction from superconducting cavities," in *Proc. 2006 Linear Accelerator Conf.*, 2006, pp. 506-510.
- [10.37] R. A. Rimmer, G. Ciovati, E. F. Daly *et al.*, "The JLAB ampere-class cryomodule conceptual design," in *Proc. 2006 European Particle Accelerator Conf.*, 2006, pp. 490-492.
- [10.38] K. Watanabe, H. Hayano, S. Noguchi *et al.*, "New HOM coupler design for ERL injector at KEK," in *Proc. 2007 Workshop RF Superconductivity*, 2007, pp. 530-535.
- [10.39] J. Sekutovicz, "Higher order mode coupler for TESLA," in *Proc. 6<sup>th</sup> Workshop RF Superconductivity*, 1993, pp. 426-439.
- [10.40] C. E. Reece, E. F. Daly, T. Elliott *et al.*, "High thermal conductivity cryogenic RF feedthroughs for higher order mode couplers," in *Proc. 2005 Particle Accelerator Conf.*, 2005, pp. 4108-4110.

- [10.41] V. Shemelin, P. Barnes, B. Gillett *et al.*, “Status of HOM load for the Cornell ERL injector,” in *Proc. 2006 European Particle Accelerator Conf.*, 2006, pp. 478-480.
- [10.42] J. Sekutowicz, A. Gössel, N. Mildner *et al.*, “Beam tests of HOM absorber at FLASH,” in *Proc. 2010 Int. Particle Accelerator Conf.*, 2010, pp. 4092-4094.
- [10.43] A. Todd, “State-of-the-art electron guns and injector designs for energy recovery linacs (ERL),” *Nucl. Instrum. Meth. A*, vol. 557, pp. 36-44, November 2006.
- [10.44] A. Arnold, H. Büttig, D. Janssen *et al.*, “Development of a superconducting radio frequency photoelectron injector,” *Nucl. Instrum. Meth. A*, vol. 577, pp. 440-454, July 2007.
- [10.45] A. Neumann and J. Knobloch, “Cavity and linac RF and detuning control simulations,” in *Proc. 2007 Workshop RF Superconductivity*, 2007, pp. 627-631.
- [10.46] F. Marhauser, “High power tests of a high duty cycle, high repetition rate RF photo-injector gun for the BESSY FEL,” in *Proc. 2006 European Particle Accelerator Conf.*, 2006, pp. 68-70.
- [10.47] J. C. Slater, “Microwave electronics,” *Rev. Modern Physics*, vol. 18, pp. 441-512, October 1946.
- [10.48] M. Liepe, W.-D. Möeller and S. N. Simrock, “Dynamic lorentz force compensation with a fast piezoelectric tuner,” in *Proc. 2001 Particle Accelerator Conf.*, 2001, pp. 1074-1076.
- [10.49] A. Neumann, W. Anders, M. Dirsat *et al.*, “CW superconducting RF photoinjector development for energy recovery linacs,” in *Proc. 2010 Linear Accelerator Conf.*, 2010, pp. 998-1000.
- [10.50] D. Schulze, “Ponderomotorische stabilität von hochfrequenzresonatoren und resonatorregelungssystemen,” Ph.D. Thesis, Kernforschungszentrum Karlsruhe, Karlsruhe, Germany, 1972.
- [10.51] A. Mosnier, “RF feedback systems for SC cavities,” in *Proc. 1998 European Particle Accelerator Conf.*, 1998, pp. 174-178.
- [10.52] P. Baudrenghien, G. Hagemann, J. C. Molendijk *et al.*, “The LHC low level RF,” in *Proc. 2006 European Particle Accelerator Conf.*, 2006, pp. 1471-1473.
- [10.53] M. Liepe, S. Belomestnykh, J. Dobbins *et al.*, “Experience with the new digital RF control system at the CESR storage ring,” in *Proc. 2005 Particle Accelerator Conf.*, 2005, pp. 2592-2594.
- [10.54] G. Kreps, A. Gössel, D. Proch *et al.*, “Excitation of parasitic modes in CW cold tests of 1.3 GHz TESLA-type cavities,” in *Proc. 2009 Workshop RF Superconductivity*, 2009, pp. 289-291.
- [10.55] E. Vogel, “High gain proportional rf control stability at TESLA cavities,” *Phys. Rev. ST Accel. Beams*, vol. 10, pp. 052001-1–052001-12, May 2007.
- [10.56] A. Salom and F. Perez, “Digital LLRF for ALBA storage ring,” in *Proc. 2008 European Particle Accelerator Conf.*, 2008, pp. 1419-1421.
- [10.57] S. Michizono, H. Katagiri, T. Matsumoto *et al.*, “Performance of digital LLRF system for STF in KEK,” in *Proc. 2008 Linear Accelerator Conf.*, 2008, pp. 1048-1050.
- [10.58] T. Allison, K. Davis, H. Dong *et al.*, “CEBAF new digital LLRF System extended functionality,” in *Proc. 2007 Particle Accelerator Conf.*, 2007, pp. 2490-2492.
- [10.59] V. Ayvazyan, K. Czuba, Z. Geng *et al.*, “LLRF control system upgrade at FLASH,” in *Proc. 2010 Personal Computers Particle Accelerator Conf.*, 2010, pp. 150-152.
- [10.60] H.-S. Kim, H.-J. Kwon, K.-T. Seol *et al.*, “LLRF control using a commercial board,” in *Proc. 2008 Linear Accelerator Conf.*, 2008, pp. 1057-1059.
- [10.61] W. L. Brogan, *Modern Control Theory*, 3rd ed., Upper Saddle River: Prentice Hall, 1991.
- [10.62] U. Meyer-Baese, *Digital Signal Processing with Field Programmable Gate Arrays*, 2nd Ed., Berlin: Springer-Verlag, 2004.
- [10.63] L. R. Dalesio, M. R. Kraimer and A. J. Kozubal, “EPICS Architecture,” in *Proc. Int. Conf. Accelerator Large Experimental Physics Control Systems*, 1991, pp. 278-282.